Journal of Power Sources 263 (2014) 338–360

Contents lists available at ScienceDirect

Journal of Power Sources

journal homepage: www.elsevier.com/locate/jpowsour

Review

Microwave-assisted synthesis of metal oxide/hydroxide composite electrodes for high power supercapacitors – A review

Soheila Faraji, Farid Nasir Ani*

Department of Thermodynamics and Fluid Mechanics, Faculty of Mechanical Engineering, Universiti Teknologi Malaysia, UTM 81310, Skudai, Johor Bahru, Johor Darul T'azim, Malaysia

HIGHLIGHTS

- Supercapacitor of metal oxide/hydroxide thin film by microwave method studied.
- Supercapacitors exhibit high specific capacitance as potential energy storage.
- Metal oxide/hydroxide films play a major role in supercapacitor technology.

ARTICLE INFO

Article history:
Received 27 January 2014
Received in revised form
28 March 2014
Accepted 30 March 2014
Available online 13 May 2014

Keywords:
Supercapacitor
Metal oxide/hydroxide
Microwave-assisted
Review

ABSTRACT

Electrochemical capacitors (ECs), also known as pseudocapacitors or supercapacitors (SCs), is receiving great attention for its potential applications in electric and hybrid electric vehicles because of their ability to store energy, alongside with the advantage of delivering the stored energy much more rapidly than batteries, namely power density. To become primary devices for power supply, supercapacitors must be developed further to improve their ability to deliver high energy and power simultaneously. In this concern, a lot of effort is devoted to the investigation of pseudocapacitive transition-metal-based oxides/hydroxides such as ruthenium oxide, manganese oxide, cobalt oxide, nickel oxide, cobalt hydroxide, nickel hydroxide, and mixed metal oxides/hydroxides such as nickel cobaltite and nickel–cobalt oxyhydroxides. This is mainly due to the fact that they can produce much higher specific capacitances than typical carbon-based electric double-layer capacitors and electronically conducting polymers. This review presents supercapacitor performance data of metal oxide thin film electrodes by microwave-assisted as an inexpensive, quick and versatile technique. Supercapacitors have established the specific capacitance (Cs) principles, therefore, it is likely that metal oxide films will continue to play a major role in supercapacitor technology and are expected to considerably increase the capabilities of these devices in near future.

1. Introduction

The electrochemical capacitor (EC) is often known and called supercapacitor [1]. As an energy storage/delivery device, supercapacitor to be of great technical potential in power systems owing to its high-power characteristics with acceptable capacity and long cycle life. Supercapacitors, sometimes called pseudocapacitors or electric double-layer capacitor (EDLC) or ultracapacitors, do not have a conventional solid dielectric. The capacitance value of an electrochemical capacitor is determined by two storage principles, both of which contribute to total capacitance of capacitor [2–4]:

(1) Double-layer capacitance (DLC) – electrostatic storage of electrical energy achieved by separation of charge in a Helmholtz double layer at the interface between surface of a conductive electrode and an electrolyte. The distance of static separation of charge in a double-layer is of the order of a few angstroms (0.3–0.8 nm), which is enormously small [3,4].
(2) Peseudocapacitance – Electrochemical storage of electrical energy with electron transfer, achieved by redox reactions with specially adsorbed ions from electrolyte, intercalation of atoms in the layer lattice or electrosorption, under potential deposition of hydrogen or metal adatoms in surface lattice sites which results in a reversible faradaic charge transfer [3,4].

The ratio of storage resulting from each opinion can vary significantly, depending on electrode design and electrolyte

* Corresponding author. Tel.: +60 7 5534715; fax: +60 7 5566159.
E-mail addresses: soheilafaraji@yahoo.com, soheilafaraji@gmail.com (S. Faraji), farid@fkm.utm.my (F.N. Ani).

http://dx.doi.org/10.1016/j.jpowsour.2014.03.144
0378-7753/

composition. Supercapacitance can enhance the capacitance value by as much as an order of magnitude over that of the double-layer by itself [3]. Supercapacitors are divided into three families, based on design of the electrodes [3–7]:

(a) Double-layer capacitors – with carbon electrodes or derivates with much higher static double-layer capacitance than faradaic pseudocapacitance.
(b) Supercapacitors – with electrodes out of metal oxides or conducting polymers with a high amount of faradaic pseudocapacitance.
(c) Hybrid capacitors – capacitors with special and asymmetric electrodes that exhibit both major double-layer capacitance and pseudocapacitance, such as lithium-ion capacitors.

In recent years, supercapacitors have attracted significant attention, mainly due to their high power density and long lifecycle [1,8]. They have the maximum available capacitance values per unit volume and the greatest energy density of all capacitors. They support up to 12,000 F/1.2 V, with capacitance values up to 10,000 times that of electrolytic capacitors. While existing supercapacitors have energy densities that are approximately 10% of a conventional battery, their power density is generally 10 to 100 times greater. Power density is defined as the product of energy density, multiplied by the speed at which the energy is delivered to the load. Greater power density results in much shorter charge/discharge cycles than a battery is capable of, and a greater tolerance for numerous charge/discharge cycles [3,9].

In order to understand the inherent differences between these two electrochemical storage systems better, supercapacitors and batteries, as well as electrochemical energy conversion systems, a Ragone plot can be drawn to demonstrate their respective performances. Ragone plots are often used to graph the characteristic power density in relation to energy density of such systems as shown in Fig. 1 [8]. The unique role that each energy storage or conversion system plays is evident by their region of dominance. While batteries are the popular choice for high portable energy storage, with Li-ion batteries achieving energy densities of 180 Wh kg^{-1} [10], the electrode materials suffer strenuous volume and irreversible phase changes during charge discharge cycling that limits their cycle-life. This disadvantage further impedes their application for high power performance applications which often require rapid charging and discharging in short intervals. These shortcomings draw attention to the characteristic strengths of ECs. Evident by Ragone plot (Fig. 1), commercial ECs do not currently possess the large energy densities of batteries, with commercial devices ranging between 5 and 10 Wh kg^{-1}. Power density of ECs far exceeds that of batteries with the ability to charge and discharge stored energy within seconds. ECs compliment this characteristic very well with a cycle life in excess of 10^6 cycles of deep discharge within a wide operational temperature range and require no further maintenance upon integration. Conscientious of environmental standards, these devices are also recyclable [11].

The electrolytes within an EC play an equally vital function in development of electrostatic and reversible redox processes necessary for charge storage and overall energy density. Choices among electrolytes range between aqueous to organic and ionic liquid, where consideration is given to electrolyte conductivity, ion size and electrochemical stability (voltage limitations). Within electrochemical capacitors, the electrolyte is the conductive connection between the two electrodes, distinguishing them from electrolytic capacitors, in which the electrolyte only forms the cathode, the second electrode. Supercapacitors are polarized and should operate with correct polarity. Polarity is controlled by design with asymmetric electrodes, or, for symmetric electrodes, by a potential applied during the manufacturing process. Supercapacitors support a broad spectrum of applications for energy and power requirements. EC was supposed to enhance the fuel cell or the battery in the hybrid electric vehicle to supply the necessary power for acceleration, and additionally allow for recuperation of brake energy. Today, several companies such as Siemens Matsushita (now EPCOS), Maxwell Technologies, Panasonic, TOKIN, ELNA, NEC and several others invest in electrochemical capacitor development [3,6,7,9,12,13].

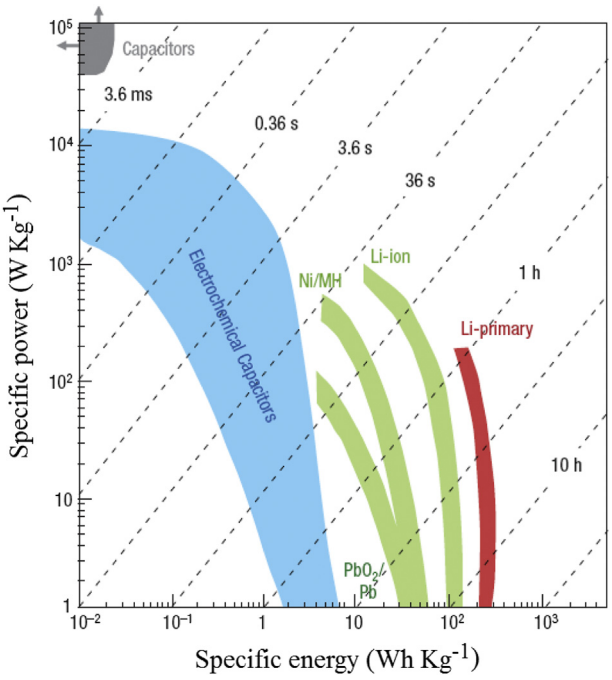

Fig. 1. Ragone plot with rough guide lines of current energy storage and conversion devices [8].

Microwaves are being in many areas of chemistry and microwave techniques have become suitable for industrial applications such as food processing [14,15] and industrial materials [16–19]. In particular, the microwave assisted technique is regarded as a novel method in synthesis of inorganic solids and is a rapidly developing area of research. This method is facile, fast, quite, secure, controllable and energy-saving. Besides decreasing synthesis time, it was duly demonstrated that microwave technique provides an effective way to control particle size distribution and macroscopic morphology in the synthesis [20]. Microwave-assisted methods have been tried to synthesize metal oxide composite electrodes as supercapacitors [21–24]. Nanostructured metal oxides, which exhibit pseudocapacitance behaviour, are considered to be excellent materials for achieving high specific capacitance.

This review presents the investigation of supercapacitive performance of metal oxide/hydroxide thin film electrode materials by microwave-assisted (MV) technique. Supercapacitors have exposed the specific capacitance (Cs) values, which are moderately comparable with bulk electrode values. Therefore, it is expected that these metal oxide thin films will continue to play a significant role in supercapacitor technology.

2. Supercapacitor

The ECs is called as supercapacitors, which occur on electrodes when the application of a potential induces faradaic current from reactions such as electrosorption or from the oxidation–reduction of electroactive materials (e.g., RuO_2, IrO_2, and Co_3O_4) [1,6,25–29].

Electrosorption occurs when chemisorptions of electron donating anion such as Cl^-, B^-, I^-, or CNS^- takes place in a process such as: $M + A^- \leftrightarrow MA^{(1-\delta)} + \delta\, e^-$. Such an electrosorption reaction of A^- an ions at the surface of an electrode, and the quantity $\delta\, e^-$ are related to the so-called "electrosorption valence" [30]. Secondly, by a replace of charge across the DL, rather than a static separation of charge across a limited distance, resulting in oxidation–reduction reactions (indicated as: $O_{ad} + ne^- \rightarrow R_{ed}$). The charge, ne^-, replaced in this reaction, and the energy storage is indirect and comparable to that of a battery. It is well known that both of two different storage mechanism of EDLC and supercapacitance exist for the supercapacitor system. Classically, one of the storage mechanisms occupies the leading position, the other is relatively weak. The comparison of EDLC and supercapacitance is showed in Table 1 [31].

2.1. Supercapacitor parameters

Supercapacitors store the electric energy in an electrochemical double layer (Helmholtz Layer) formed at a solid electrolyte interface. Positive and negative ionic charges within the electrolyte accumulate at the surface of the solid electrode and compensate for the electronic charge at the electrode surface. The thickness of the double layer depends on the concentration of the electrolyte and on the size of the ions and is in the order of 5–10 Å, for concentrated electrolytes. The double layer capacitance is about 10–20 μF cm^{-2} for a smooth electrode in concentrated electrolyte solution and can be estimated according to Eq. (1) [12];

$$C = \varepsilon_0 \varepsilon_r A/d \text{ or } C/A = \varepsilon_0 \varepsilon_r/d \quad (1)$$

assuming a relative dielectric constant of 10 for water in the double layer and d being the thickness of the double-layer with surface area A. The corresponding electric field in the electrochemical double layer is very high and assumes values of up to 10^6 V cm^{-1} easily. Compared to conventional capacitors where a total capacitance of pF and μF are typical, the capacitance and energy density stored in the electrochemical double layer are rather high per se and the idea to build a capacitor based on this effect is tempting. In order to achieve a higher capacitance the electrode surface area is additionally increased by using porous electrodes with an extremely large internal effective surface. Combination of two such electrodes gives an electrochemical capacitor of rather high capacitance. Fig. 2 [12] presents a schematic diagram of an electrochemical double-layer capacitor consisting of a single cell with a high surface-area electrode material, which is loaded with electrolyte. The electrodes are separated by a porous separator, containing the same electrolyte as the active material. The potential drop across the cell is also shown in Fig. 2. It also shows that charges can be stored and separated at the interface between the electrolyte and the conductive solid particles (such as carbon particles or metal oxide particles). This interface can be treated as a capacitor with an electrical double-layer capacitance. The double layer capacitance, Cdl, at each electrode interface is given by Refs. [1,6];

$$Cdl = \varepsilon A/4\pi t \quad (2)$$

where ε is the dielectric constant of the electrical double layer region, A the surface area of the electrode and t is the thickness of the electrical double layer. The specific energy (E) and specific power (P) of supercapacitors are calculated according to Refs. [1,6];

$$E = (1/2)CV^2 = QV/R \quad (3)$$

$$P = V^2/4R \quad (4)$$

where C is the dc capacitance in Farads, V the nominal voltage, and R is the equivalent series resistance (ESR) in ohms (Ω) [1,32]. Also Q indicates the stored total charges in coulombs. From these two equations, it can be seen that C, V and R are three important variables determining the performance of supercapacitor. In general, the capacitance and stored charge basically depend on the electrode material used [1].

The specific capacitance (C_s), with a unit of Faraday per gram (F g^{-1}) can be obtained by the Eq. (5) [1];

$$C_s = C_i/W \quad (5)$$

where W is the weight in grams of the electrode material in the electrode layer, and C_i is the electrode capacitance (anode or cathode). Note that this specific capacitance is the intrinsic capacitance of the material. A higher specific capacitance does not necessarily mean that this material will be a better supercapacitor electrode material, because electrode capacitance is also strongly dependent on the electrode layer structure, the electron and ion transfers within the layer [1].

If the charge (Q) in Eq. (5) accumulated inside the electrode layer is calculated using the area under the cyclic voltammogram in either direction in a potential window from E_1 to E_2, the capacitance, C_i (=positive or negative capacitance), of this electrode layer can be measured by Eq. (6) [1]:

$$C_i = |Q/(E_2 - E_1)| \quad (6)$$

In addition to cyclic voltammetry, electrochemical impedance spectroscopy (EIS) is also a functional tool for determining the capacitance of ES materials [1]. The most popular way to run EIS measurements is collecting the ES impedance data at the open-circuit potential by applying a small amplitude of alternative interrupting potential (e.g., ±5 to ±10 mV) over a wide range of frequency f (e.g., 1 mHz–1 MHz). It can provide the relationship between the imaginary part of impedance $|Z|$ and f. The capacitance can be calculated using $C = 1/(2\pi f|Z|)$ using a linear portion of a log $|Z|$ *vs.* log f curve, which is called the Bode plot. This Bode plot shows that the capacitance decreases with increasing frequency, and at the high frequency region the supercapacitors behave like a pure resistance, indicating that the electrolyte ions probably cannot penetrate into micropores under high frequencies. The EIS can also be expressed as a Nyquist diagram, where the imaginary part of impedance, $Z(f)''$, is plotted against the real part of impedance, $Z(f)'$

Table 1
Comparison between electric double-layer capacitors (EDLC) and supercapacitance [31].

	EDLC	Supercapacitance
1.	Non-faradaic	Involves faradic process(es)
2.	20–50 μF cm^{-2}	2000 μF cm^{-2} for single-state process; 200–500 μF cm^{-2} for multi-state, overlapping process
3.	C fairly constant with potential, except through the potential of zero charge	C fairly constant with potential for RuO_2; for single-state process; exhibits marked maximum
4.	Highly reversible charging/discharging	Can exhibit several maxima for overlapping; multi-state processes, as for H at Pt, quite reversible but has intrinsic electrode-kinetic rate limitation determined by R_f
5.	Has restricted voltage range (contrast non-electrochemical electrostatic capacitor)	Has restricted voltage range
6.	Exhibits mirror-image voltammograms	Exhibits mirror-image voltammograms

[7]. From the Nyquist plot, a charge transfer resistance can be obtained from the diameter of the semicircle on this plot. At high frequency (larger than 104 Hz), the impedance implies the conductivity of both active materials and electrolyte. The high-to-medium frequency region (10^4–1 Hz) shows pseudocharge transfer resistance, which is associated with the porous structure of the electrodes. At low frequency ranges (less than 1 Hz), the impedance plot is the characteristic feature of pure capacitive behaviour. Theoretically, a pure capacitor should display a parallel line to the imaginary axis of the Nyquist plot. In normal cases, the plot shows a line with the inclined angle between 45° and 90° against the real axis, corresponding to the ion diffusion mechanism between Warburg diffusion and ideal capacitive ion diffusion (pseudocapacitance) [33]. This deviation from the parallel line may be attributed to two reasons: one is the different penetration depth of the alternating current signal in virtue of pore size distribution at both electrodes, leading to abnormal capacitance, the other is the redox reaction at the electrode, giving rise to pseudocapacitance [34].

In Fig. 3 [12] the impedance plane representation (Nyquist plot) of an ideal capacitor and a simplified electrochemical capacitor, both having the same ESR (equivalent series resistance at 1 kHz), are compared. While the ideal capacitor exhibits a vertical line, the supercapacitor starts with a 45° impedance line and approaching an almost vertical line only at low frequencies. The non-vertical slope of the low frequency impedance of any real electrochemical capacitor can be easily reproduced in any model equation by replacing the capacitance expression with a constant phase element (CPE) expression. This amounts to replacing every $j\omega$ (j – imaginary unit, ω – angular frequency) expression with $(j\omega)^p$, where $0 < p < 1$, and where $p = 1$ represent an ideal capacitor with no frequency dependence. This non-ideality is a typical feature of electrochemical charging processes, and may be interpreted as resulting from a distribution in macroscopic path lengths (non-uniform active layer thickness) [25] or a distribution in microscopic charge transfer rates [26], adsorption processes, or surface roughness. The 45° region (Warburg region) is a consequence of the distributed resistance: capacitance in a porous electrode. At higher frequencies the resistance as well as the capacitance of a porous electrode decreases, because only part of the active porous layer is accessible at high frequencies. The supercapacitor may thus be represented by an ideal capacitor with an ESR increased by the equivalent distributed resistance (EDR).

2.2. Supercapacitors performance characterization

Quantifying the developed capacitance in ECs is basic for the assessment of characteristic parameters (i.e. power and energy density), and to present the knowledge of where tested materials

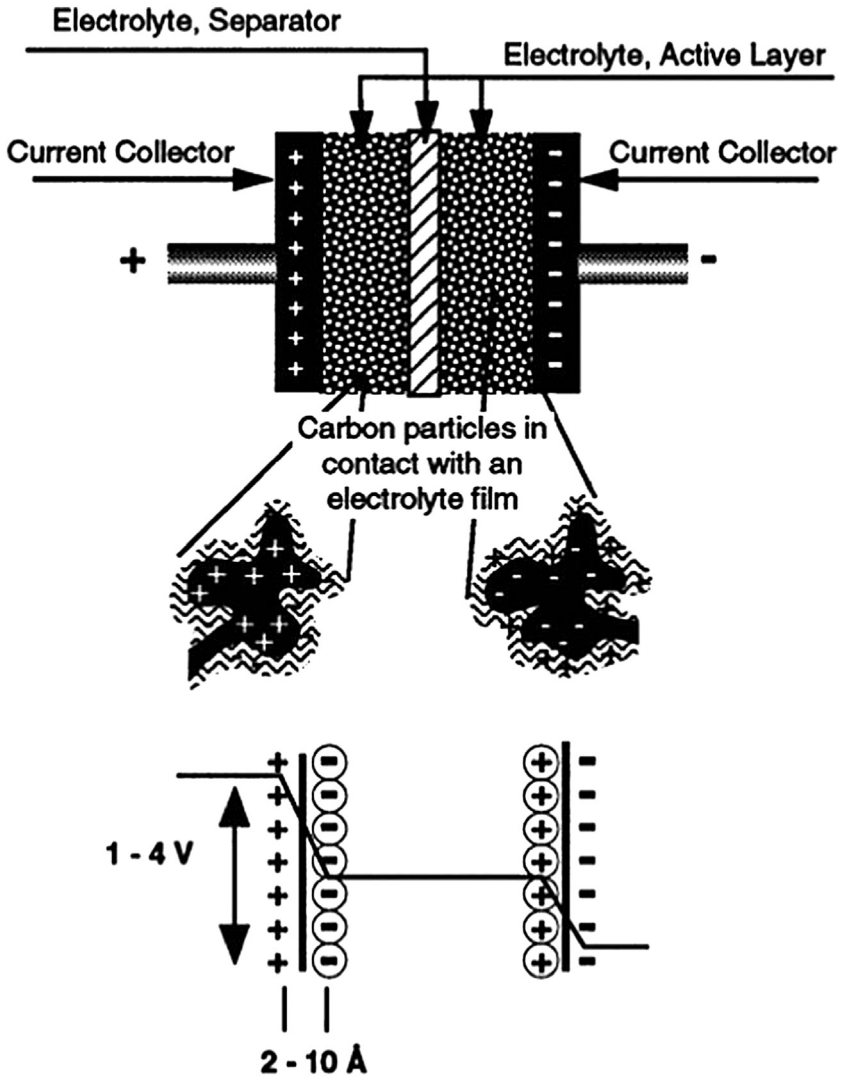

Fig. 2. Principle of a single-cell double-layer capacitor and illustration of the potential drop at the electrode:electrolyte interface [12].

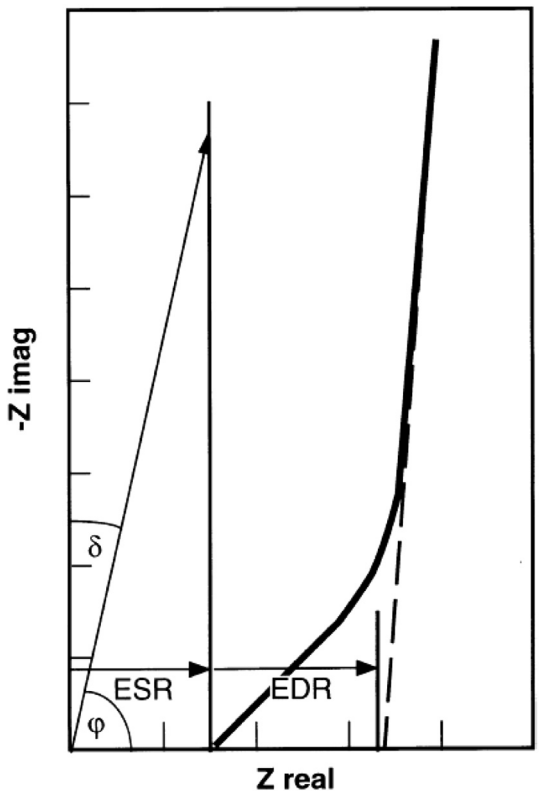

Fig. 3. Schematic representation of the Nyquist impedance plot of an ideal capacitor (vertical thin line) and an electrochemical capacitor with porous electrodes (thick line) [12].

would suitably fit in terms of application. Trouble-shooting the design of materials or device constructions also benefits from such performance testing. In addition to the determination of capacitance, power and energy characteristics, the stability testing and self-discharge tendency of an electrode material for cycle-life and reliability is necessary to consider for the commercial pursuit of any designed material [9].

Charging rates, voltage ranges, and methods for calculation of metrics also affect the reported results and should closely match currently established and accepted procedures used for packaged cells of supercapacitors. The primary performance metrics for packaged supercapacitors include gravimetric energy and power densities, and lifecycle testing [35]. In turn, a supercapacitor's energy density (Wh kg^{-1}) is primarily determined by the cell's electrode material and electrochemical voltage window. With energy density currently the primary limitation for supercapacitors, the most important metric for an electrode material is thus its specific capacitance (F g^{-1}). A supercapacitor's power scales with the square of voltage divided by its ESR [36]. The measured ESR of a test cell, as well as that of a full scale packaged capacitor, is due to all cell components (leads, current collectors, electrodes, electrolyte, and separator) and therefore only a portion of the measured resistance can be attributed to the electrode material itself. Other metrics, such as an electrode material's energy and power density, also do not correlate directly to those of a packaged cell and must include information such as package dimensions and the mass of the other cell components to be meaningful. Specific capacitance is the capacitance per unit mass for one electrode Eq. (7);

$$C_s\left(\mathrm{F\,g^{-1}}\right) = 4 \times C/m \tag{7}$$

where C is the measured capacitance for the two-electrode cell and m is the total mass of the active material in both electrodes. The multiplier of 4 adjusts the capacitance of the cell and the combined mass of two electrodes to the capacitance and mass of a single electrode. If volume is more important for the targeted application, the electrode material's volume may be substituted for mass. Cell capacitance is best determined from galvanostatic or constant current (CC) discharge curves using Eq. (8) with I the discharge current and

$$C = I/(\mathrm{d}V/\mathrm{d}t) \tag{8}$$

$\mathrm{d}V/\mathrm{d}t$ calculated from the slope of the CC discharge curve. Galvanostatic discharge is the accepted measurement method for determining capacitance for packaged supercapacitors in the supercapacitor industry and correlates more closely to how a load is typically applied to a supercapacitor in the majority of applications. The same voltage range should be used for testing should match that used for commercial cells and should reflect the electrolyte's electrochemical window from 0 V to approximately 1 V for aqueous electrolytes and from 0 V to 2.5–2.7 V for organic electrolytes [36]. Maximum voltages for hybrid cells will depend upon electrode materials and electrolytes. The initial portion of a discharge curve exhibits an IR drop due to internal resistance and the rest of the curve will typically be linear for non-faradic materials. Supercapacitive and hybrid systems can exhibit large deviations in linearity based upon varying capacitance with voltage. Fig. 4 [37] illustrates CC charge–discharge curves (100 mA g^{-1}) of an asymmetric manganese oxide/activated carbon ultracapacitor in 2 mol L^{-1} KNO_3 electrolyte cycled at different maximum cell voltages. When the maximum voltage is at 2.2 V, the CC curve is no longer symmetric indicating noncapacitive behaviour. Therefore, in order to find the optimal cell voltage, the coulombic efficiency (η) was calculated as:

$$\eta = q_d/q_c \tag{9}$$

where q_d and q_c are the total amount of discharge and charge of the capacitor obtained from the galvanostatic experiments presented in Fig. 4.

Fig. 5 [37] demonstrates, for the same cell, the coulombic efficiency and specific capacitance (F g^{-1}) *vs.* maximum voltage. While the specific capacitance continues to increase with increasing voltage range, the coulombic efficiency decreases dramatically when cycled above 2 V. Driving a cell above its true maximum operating voltage can lead to an overestimation of specific capacitance and cells operated at these levels will have shortened

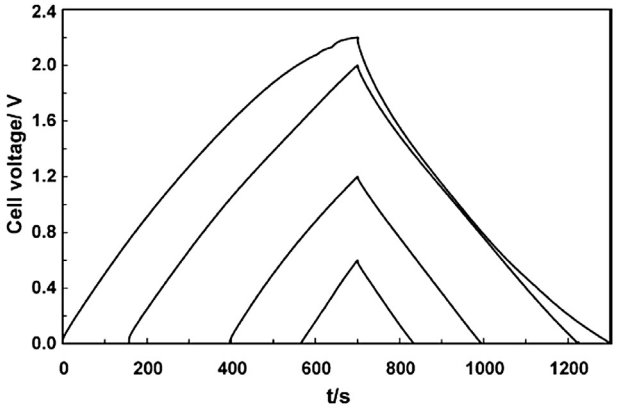

Fig. 4. CC charge–discharge curves (100 mA g^{-1}) of an asymmetric manganese oxide/activated carbon ultracapacitor in 2 mol L^{-1} KNO_3 electrolyte [37].

lifetimes and poor efficiencies due to the non-reversible reactions within the cell. Significant errors can also be introduced by the method used to calculate the slope (dV/dt). As stated previously, capacitance varies with voltage, especially for hybrid and supercapacitive cells, and it is important to calculate capacitance using the typical operating voltage range for the application that the device will be used. Most supercapacitors will be operated in the range of V_{max} to approximately $½V_{max}$ and the recommended method is to use two data points from the discharge curve with $dV/dt = (V_{max} - ½V_{max})/(T_2 - T_1)$. Including the lower half of the voltage range in the calculations can distort the apparent capacitance above that which is practically realizable for an actual application [36].

Very low rates of discharge also lead to large errors, especially when coupled with small electrode masses, with the current from cell leakage, capacitance from other cell components, and faradic reactions contributing an increasing percentage of the signal as discharge rate and electrode mass are decreased. Charge and discharge rates should be specified in units of current per electrode mass with the duration of charge and discharge corresponding to typical supercapacitor applications. Current should be adjusted to provide charge and discharge times of approximately 5–60 s. For example, a test cell with two 10 mg electrodes composed of 100 F g^{-1} specific capacitance material will have a capacitance of 0.5 F. With a discharge current of 40 mA, corresponding to a discharge density of 4 A g^{-1}, discharge time from 2.7 to 0 V will be approximately 34 s [36].

Fig. 6 [37] presents the Nyquist plots for the three kinds of capacitors. The equivalent series resistance (ESR) can be extracted from the high frequency (10 kHz) part of the curves. As it could be expected, the ESR of the symmetric manganese oxide (MnO_2) capacitor is higher than the ESR obtained for the symmetric activated carbon (AC) capacitor, due to the differences in conductivity of the two-electrode materials. However, when an asymmetric system is built by combining the two materials, the ESR is close to the value for activated carbon one. Fig. 6 also shows that at low frequency, the imaginary part of the impedance curves approaches, in all cases, to a vertical line indicating a capacitive behaviour. Table 2 [37] summarises the data obtained from the impedance spectroscopy experiments presented in Fig. 6, such as the resistance (ESR) and the time constant (t_d), together with the data given by cyclic voltammetry performed on the same cells, such as the maximum cell voltage (V_{max}) and the specific capacitance (C_s). In addition, the specific energy (E) was calculated by using Eq. (3) and the maximum specific power (P_{max}) was calculated according to Eq. (7);

$$P_{max} = V_{max}^2 \Big/ 4\mathrm{ESR} \times m \tag{10}$$

where m is the total mass of both electrodes (including binder and conductivity agent). After analysing all the data contained in Table 2 [37], it is possible to conclude that the performance of the hybrid capacitor is much better than for any of the symmetric systems. In particular, the specific energy, which can be extracted from the asymmetric manganese oxide/activated carbon capacitor, is 5–10 times higher than for a symmetric system working in the same aqueous medium.

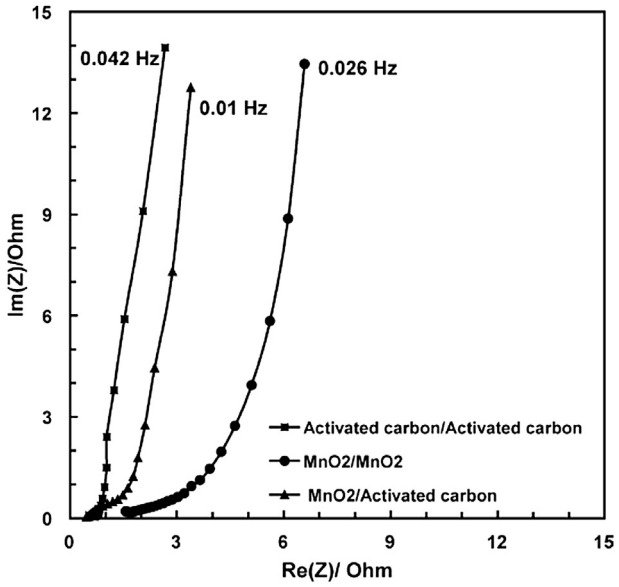

Fig. 6. Nyquist plots of the symmetric manganese oxide/manganese oxide and activated carbon/activated carbon capacitors and of the asymmetric manganese oxide/activated carbon capacitor. Electrolyte 2 mol L^{-1} KNO_3 in water [37].

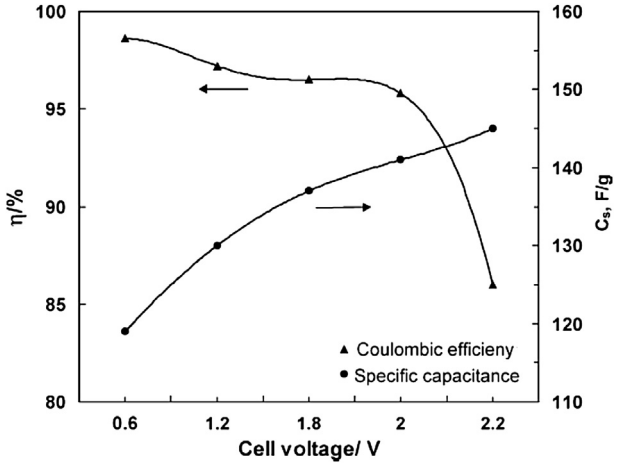

Fig. 5. Coulombic efficiency and specific capacitance (F g^{-1}) of an asymmetric manganese oxide/activated carbon supercapacitor in 2 mol L^{-1} KNO_3 electrolyte *vs.* the cell voltage [37].

2.3. Supercapacitor types and their electrode materials

Supercapacitors can be made from different materials, depending on the type of energy storage required by the application at hand and the required capacitance ranges. The electrode materials for supercapacitors can be classified into three types based on their usage for EDLCs, pseudocapacitors, and hybrid supercapacitors (Table 3) [38]. A major number of materials are currently available for supercapacitors; the significant commercial material is carbon, which is extensively used and can be converted into many forms. Other materials include metal oxides such as ruthenium, manganese nickel, cobalt, and iron. Conducting

Table 2
Comparative performance obtained from impedance spectroscopy and cyclic voltammetry experiments on the symmetric manganese oxide/manganese oxide and activated carbon/activated carbon capacitors and on the asymmetric manganese oxide/activated carbon capacitor [37].

Electrode material (±)	ESR at 10 Hz (Ω)	t_d (s)	V_{max} (V)	C_s (F g^{-1})	E (Wh kg^{-1})	P_{max} (kW)
AC/AC	0.44	0.34	0.7	180	3.6	51
MnO_2/MnO_2	1.56	0.81	0.6	160	1.9	3.8
MnO_2/AC	0.54	0.26	2	140	21.0	123

polymers have also been employed in supercapacitors. Supercapacitors are gradually more based on carbon nanotubes (CNTs). The use of CNTs and other nanomaterials allows for an important and major increase in surface area, among other advantages. The other types of generally used supercapacitor materials are composites obtained by combining two or more component materials. The composites can include a nanomaterial. For example, CNTs with metal oxides or conducting polymers formed as a composite. For the supercapacitor electrodes, there is an interest in nanostructured materials that have improved capacitive performance characteristics and increased surface area. The synthesis of nanoengineered materials is now recognized as a main factor in developing high performance supercapacitor devices [6,7,38].

2.4. Comparison of electrochemical capacitors (ECs) and batteries

Since ECs store electrical charge only at the electrode surface, rather than within the entire electrode, they tend to have lower energy densities compared to batteries. The charge–discharge reaction is not limited by ionic conduction into the electrode bulk, therefore ECs can be run at high rates and provide high specific power. In addition, most of the EC materials do not participate in redox reactions, so there is little deterioration in the electrode, which has good cycle characteristics, and maintenance is unnecessary. Due to such differences, the corresponding electrochemical behaviour is also different. It was reported that the energy density of EC is 10 times higher than electrostatic capacitor [3]; in addition, EC has the advantages of high power density, short charge–discharge time, high charge–discharge efficiency, long cycle life, wide range of operating temperatures, environmental friendliness, and safety compared with battery [1,3,6].

2.5. Challenges for supercapacitors

Although supercapacitors have many advantages over batteries and fuel cells, they also face some challenges at the current stage of technology such as (1) low energy density, (2) high cost, (3) high self-discharging rate, and (4) industrial standards for commercialization [1]. Although this kind of supercapacitor is commercially available, it is necessary to establish some general industrial standards such as performance, electrode structure, electrode layer thickness and porosity and so on. Due to the variety of applications as well as limited commercial products. It has not still been able to search out generally available industrial standards for ES at this moment [1]. Therefore, it is necessary to put some effort on ES standard establishment for different applications.

In some ways similar to the challenges faced by portable electronic devices, hybrid electric vehicles (HEVs) require a high power energy source. While oversized battery systems have been used to meet the power demands, difficulties arise in managing the generated heat resulting from exothermic reactions and resistances, as well as having to adopt a predictable low cycle life. By reducing the size of the battery and/or the major energy supplier, ECs can also efficiently help meet the irregular stop-and-go power require intervals of HEVs in urban settings. Serving to capture the break energy from these intervals, their fast recharge periods and high cycle efficiency (>95%) are well suited to develop the fuel efficiency of HEVs. A review [13] supported EC use in HEVs by comparing current high power lithium ion batteries and ECs to estimate the relevant energies captured and available for immediate use. Contrary to the conventional perspective, in a charge time of 10 s or less the ECs possess roughly twice the energy density compared with high power batteries, and do not have need for a heat management system with high rate cycling. Other transport systems that stand to gain in energy efficiency through EC incorporation include buses, trams, and trains.

The valuable contributions made by ECs are becoming increasingly apparent as society and technology trends continue to focus on employing alternative and ecologically mindful energy generation and storage systems. In particular, with industry and government regulations continuing to press for green energy and product solutions, ECs have an advantage over batteries with respect to a longer life-span and material recyclability. Despite this, challenges related to their low energy density and high costs deter consumer investment and inhibit their market strength. Two concurrent strategies to employ this problem have focused on developing ionic liquid electrolytes as a safe, stable option with a broad operating voltage (>3 V) and advancing electrode materials to enhance capacitive charge storage. The latter, in particular, has capable developments ranging from the appreciation of sub-nanopores for modelling to the enhanced performances resulting from nanocomposite electrodes and hybrid system designs [9].

A force in research to optimise both hybrid materials EDLC and supercapacitance systems is expected to make success in combining rapid capacitive charging with high energy density. Progressive exploration towards the combination of carbon with redox materials (metals oxides) to develop and increase capacitive ability appears beneficial; however understanding the main effects of pore size distribution together with stability and effective material usage remain necessary and production methods remain equally significant for any practical purpose, where a simple, direct procedure is required for commercial translation.

2.6. Application of supercapacitors and future works

As a developing technology for energy storage, ECs are still achievement recognition for their use, and continue to broaden their application towards new fields. Historically used as simple devices for memory actuator and back-up applications [12], the improvements made in electrode materials to enhance high EDLC and supercapacitance and the potential they propose in asymmetric and hybrid designs have been comparatively recent since their commercialisation. At present, commercial capacitors continue to represent the benefits ECs have in providing high-power energy storage and long life.

A number of applications for which ECs are currently employed make use of their high pulse power to supply energy in very short time periods (ms-s). Serving as a power source to keep against power disturbances or propose low energy for extended periods of time, they have been incorporated into products ranging from cameras, computers, and mobile phones to energy generator systems used in avoiding costly system shut downs and production loss. The benefits to support their use over secondary-batteries are validated by faster charge times and a considerably longer cycle life that endures a negligible loss in performance with time. The isolated usage of ECs in domestic electronics has also been exposed

Table 3
Classification of supercapacitor types and their electrode materials [28].

Supercapacitors	Electrode materials
Electric double layer capacitors	• Carbon aerogels • Activated carbon • Carbon fibers • Carbon nanotubes
Pseudocapacitors	• Metal oxides • Conducting polymers
Hybrid capacitors ◦ Asymmetric ◦ Composite ◦ Battery-type	• Carbon materials, conducting polymers • Carbon materials, metal oxides

successful with marketed power tools that aim the average homeowner. These are designed for an expected infrequent and short-period use that is well addressed by ECs in having a 90 s recharge time and seemingly unlimited cycle-life. The dependability of EC technology has also been supported by their use in the emergency doors of the Airbus A380 and electromechanical actuators for engine ignition, placing them to occupy critical operations. Systems that integrate both ECs and batteries for synchronous use in a hybrid design complement these two energy devices by developing their effective strengths. Portable energy systems can promote from this design by reducing the battery size to address small average load demands, while short infrequent high power pulses are met by the EC. Additionally, reducing the average energy demands can conversely raise the life span of the battery. Such systems aid producers of portable electronics and mobile telecommunications in their quest to frequently miniaturise their products [39].

Nowadays, industrial and commercial ECs are accessible from a number of countries, such as Japan and Russia, USA, and most of capacitors are EDLCs. Powerstor, Maxwell, Evans and Los Alamos National Lab in USA had done large quantity work of ECs. The products which produced by NEC Tokin and Panasonic company (Japan) occupy a large market share ECs fields; the Eocnd company of Russia has considered the ECs for 30 years, which characterizes the highly developed level of Russia in capacitors' fields. In addition, other important companies occupied in increase of ECs are SAFT in France, Cap-xx NESS [40] in South Korea and in Australia. The ECs used in electric vehicles have been listed to advance plan in Tenth Five years Plan. Industrial and commercial companies such as EPCOS [41], Maxwell [42], and Panasonic [43] presently manufacture the common of their electrochemical supercapacitors using symmetric activated carbon electrode materials and an acetonitrile electrolyte. The performance characteristics of several commercial ECs are manufactured by the past noted companies and others. Current markets address a large majority of their energy demands for portable applications with batteries as a result of their large energy densities in contrast to their light weight and small volume. Unbeneficial in allowing ECs to mirror a similar market power, their low energy density largely confines them to applications requiring short peak power pulses. Efforts in industry and academic research alike are devoting important attention to the enlargement of novel materials and electrolytes to attempt this shortcoming, which together with the current costs of these devices are the chief inhibitors of ECs in broadening their combination in current electrical systems.

By meeting performance objectives, future ECs is expected to realize energy densities that advance that of current batteries with an insignificant loss to their power density. In addition, a development in the energy storage would help improve market application, and give a cost saving according to the reduction in necessary materials for device fabrication. The assessable success of these efforts will have a major impact on the future request of these high power energy storage devices, and their contribution toward developing the energy efficiency and life span of their adapted systems.

3. Microwave

Since World War II, there have been major developments in the use of microwaves for heating applications. After this time it was recognized that microwaves had the potential to offer rapid, energy-efficient heating of materials. Microwave applications in mining and process metallurgy have been the subject of many research studies over the past two decades. The major applications of microwave heating, today include food processing, wood drying, plastic and rubber treating as well as curing and preheating of ceramics [14,16,44]. As a simple, quick, inexpensive, uniform and energy efficient heating method, microwave irradiation has been widely used in the industry and academia to synthesize such materials as porous materials [45], inorganic complex [46], nanocrystalline particles [47] and organic compounds [48]. The application of microwave energy to the processing of various materials such as metals, composites, and ceramics presents several advantages over conventional heating methods. These advantages include unique microstructure and properties, enhanced product yield, energy savings, reduction in manufacturing cost and synthesis of new materials [44]. Microwave heating is fundamentally different from the conventional one in which thermal energy is delivered to the surface of material by radiant and/or convection heating that is transferred to the bulk of material via conduction. In contrast, microwave energy is delivered directly to the material through molecular interaction with the electromagnetic field. Microwave heating is the transfer of electromagnetic energy to thermal energy and is energy conversion rather than heat transfer. Since microwaves can go through the material and provide energy, heat can be generated throughout the volume of the material resulting in volumetric heating. Hence, it is possible to realize fast, quick and uniform heating of thick materials. Therefore, the thermal gradient in the microwave-processed material is the reverse of that in the material processed by conventional heating. In conventional heating, slow heating rates are selected to reduce steep thermal gradient leading to process-induced stresses. Thus, there is a balance between product quality and processing time. During microwave processing, the potential survives to reduce processing time and improve product quality as microwaves can transfer energy throughout the whole volume of the material. In this case, energy transfer arises at a molecular level that can have some extra advantages. When microwave energy is in contact with materials having different dielectric properties, it will selectively couple with the higher loss tangent material. Hence, microwaves can be used for the selective heating of the materials [44]. Universally, the microwave-assisted hydrothermal synthesis (MAHS) method is a homogeneous heating process and constructs the possibilities in obtaining new and modified forms of materials through the direct energy transfer from the water molecules to the precursors in comparing with conventional hydrothermal synthesis. The advantages of microwave-assisted hydrothermal process over conventional hydrothermal method are (a) extremely rapid kinetics of crystallization, (b) very rapid heating to the required temperature and (c) possible formation of new meta-stable phases. Such a unique "molecular heating" method has been shown to supply several merits in materials preparation, e.g., rapid volumetric heating, high reaction rate, short reaction time, high reaction selectivity, and energy saving. Microwave-assisted hydrothermal/solvothermal methods have been tried to fabricate metal oxides although they have been extensively applied to organic synthesis [48]. Subsequently, it is still lack of detailed discussion on the fabrication of metal oxides through such interesting methods [49,50]. This review focuses on the latest developments and the current status of research on metal oxides/hydroxides composite electrodes by microwave processing.

3.1. Characteristics of microwaves and dielectric heating

Microwaves are electromagnetic radiation, whose frequencies lie in the range of 0.3–300 MHz between radio frequencies and infrared radiation. Only narrow frequency windows centred at 900 MHz and 2.54 GHz are approved for microwave heating purposes. Microwave energy is a non-ionizing radiation that causes molecular motion by migration of ions and rotation of dipoles, but

does not cause changes in molecular structure because it corresponds to excitation of rotational motion of molecules. An understanding of the microwave interaction with materials has been mostly based on concepts of dielectric heating and of the resonance absorption due to rotational excitation [51]. Thus energy transfer from microwaves to the material is believed to occur either through resonance or relaxation, which results in rapid heating. The accurate nature of microwave interaction with reactants in the synthesis of inorganic solids is somewhat unclear yet. The fundamental theory underlying microwave dielectric heating has been well summarized in several reviews and books [51]. Microwave frequencies correspond to rotational excitation energies in materials. Hence, the incident microwaves excite rotational modes in a material and the energy absorption occurs by resonance. The absorbed energy may be completely dissipated as heat during de-excitation via internal mode coupling. The role of microwave irradiation in chemical reactions can be readily appreciated because the regime of rotational–vibrational excitations is essential for chemical reactions.

Microwave energy is classically lost to the sample by two mechanisms [51]: dipole rotation and ionic conduction. In many practical applications of microwave heating, dipole rotation and ionic conduction occur concurrently. Dipole rotation refers to the alignment, due to the electric filed, of molecules in the sample that have permanent or induced dipole moments. Ionic conduction is the conductive migration of dissolved ions in the applied electromagnetic field.

3.2. Interaction of microwaves with materials

It is known that the interaction of dielectric materials with microwaves leads to what is commonly illustrated as dielectric heating due to dipole rotation. Dielectric heating in microwaves can take place either using resonance modes of absorption, or using relaxational mechanisms as a result of phase lag between the motion of the polar species in the material and alternating microwave field [51]. Mingos and Baghurst [52] have described the factors which play a role in microwave heating: (1) superheating in the presence of a large number of ions; (2) more rapid achievement of the reaction temperature and (3) efficient mixing and boundary effects. A suitable assess of the heating effect which occurs in an applied field is $\tan \delta = \varepsilon''/\varepsilon'$ is the phase difference between the polarization of the material and the electric field. In materials where the dipoles rotate freely, such as in liquids, the rotational frequency of the dipole establishes the dissipation of energy from the applied field. In general, the dipolar species in any medium possesses a characteristic relaxation time, t, and the dielectric constant is, therefore, frequency-dependent. This is expressed by representing the dielectric constant as a complex quantity, $\varepsilon^* = \varepsilon' + i\,\varepsilon''$, where ε' and ε'' are the real and imaginary parts of the dielectric constant. The dielectric constant is a measure of a sample's ability to obstruct the microwave energy as it passes through, and the loss factor measures the sample's ability to dissipate that energy [20]. The word "loss" in the loss factor is used to indicate the amount of input microwave energy that is lost to the sample by being dissipated as heat. When microwave energy penetrates a sample, the energy is absorbed by the sample at a rate dependent upon its dissipation factor.

Magnetic polarization may also contribute to the heating effect observed in materials with magnetic properties [20]. The dielectric relaxation time is defined as the time that it takes for the molecules in the sample to achieve 63% of their return to disorder. The loss tangents of the molecules, which may be related to the ability of the solvent to absorb energy in a microwave cavity, depend on the relaxation times of the molecules. These relaxation times depend critically on the nature of the functional groups and the volume of the molecule. It is interesting that functional groups capable of hydrogen bonding have a particularly strong influence on the relaxation times [51]. It has been reported that microwave dielectric heating has the following advantages compared to conventional heating for chemical conversions [51]; (a) the introduction of microwave energy into a chemical reaction which has at least one component which is capable of coupling strongly with microwaves can lead to much higher heating rates than those which are achieved conventionally; (b) there is no direct contact between the energy source and the reacting chemicals because the microwave energy is introduced into the chemical reactor remotely; (c) it is volumetric and instantaneous (or rapid) heating with no wall or heat diffusion effects; (d) it is specific and selective heating because chemicals and the containment materials for chemical reactions do not interact similarly with the generally used microwave frequencies for dielectric heating; (e) these selective interactions mean that microwave dielectric heating is an ideal method for accelerating chemical reactions under increased pressure conditions [52].

3.3. Microwave equipments for materials synthesis

The typical microwave instrument for materials synthesis is the same one used for heating analytical samples. It consists of six main components [52]: the microwave generator (called the magnetron), the waveguide, the microwave cavity, the mode stirrer, a circulator, and a turntable as shown in Fig. 7 [52]. The magnetron is a device for generating fixed frequency microwaves, which is principally thermionic diode with heated cathode acting as sources of electrons. From the magnetrons the microwaves are commonly directed toward a target placed in microwave cavities with the use of waveguides, which are usually made of sheet metal. Then it is injected directly into the microwave cavity where the mode stirrer homogeneously distributes the incoming energy in various directions. The percentage of the incoming energy that is absorbed depends upon the sample size and dissipation factor. Many microwave preparations reported in the literature have all been made with the use of domestic microwave ovens operating at 2.45 GHz (this corresponds to a relaxation time of 65 ps) and with a maximum output power of 1 kW. Materials fall into three categories, with respect to their interaction with microwaves [53]; (a)

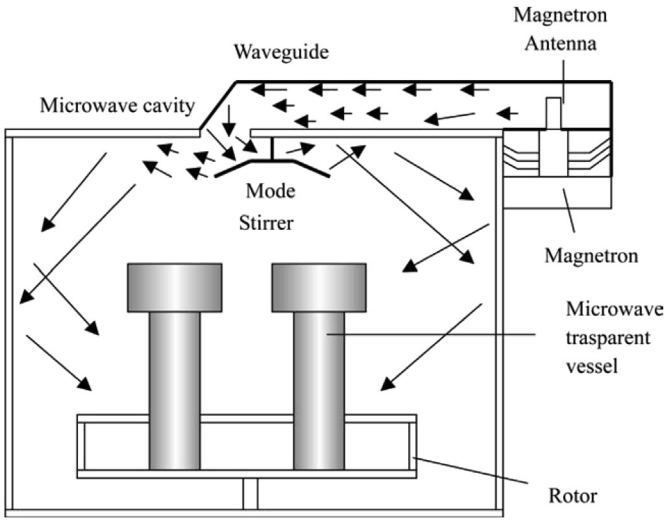

Fig. 7. Schematic illustration of microwave equipment for the synthesis of inorganic materials [52].

microwave reflectors (metals), which are therefore used in making waveguides; (b) microwave transmitters which are transparent to microwaves (low-loss materials), typified by teflon and fused quartz; they are therefore employed for containers for carrying out synthesis and chemical reactions in microwaves; and (c) microwave absorbers (high-loss materials) which constitute the most important class of materials for microwave synthesis; they take up the energy from the microwave field and get heated up very rapidly. In microwave synthesis of materials, the precursor solutions used are absorptive materials and the materials used for construction of the primary components of microwave units are reflective materials, e.g., Teflon polymer. Microwave ovens for research can be designed for monitoring parameters such as temperature and pressure while heating a sample in the microwave. For monitoring systems, the only limitation is that the measuring probes must not perturb the microwave energy.

3.4. Comparison of microwave-assisted supercapacitor synthesis and other methods

There are several different, important methods to synthesize supercapacitor materials. They include electrochemical deposition, chemical bath deposition, chemical vapour deposition, sol–gel and the microwave assisted method [38].

The most basic form of electrochemical deposition is the electrodeposition method, in which a coating or film of material is produced on a surface by the action of electric current. The benefits of the electrodeposition method include mass production, low capital investment costs, and precise control on parameters such as film thickness, deposition rate and uniformity [54–56]. Chemical bath deposition (CBD) is a low temperature technique that allows for relatively inexpensive deposition of material on large area substrates. The CBD method involves the direct deposition of a material from a solution medium without the application of current or voltage. CBD occurs on a substrate immersed in a solution by means of a reaction from the solution containing different precursors dissolved either in ionic or molecular form. These react chemically on the substrate, resulting in film formation by nucleation. Additionally, the relatively low cost, large substrate area, and low temperature processing of CBD, another advantage is its relative simplicity, particularly when compared to electrodeposition [57]. In its simplest form, the chemical vapour deposition (CVD) process is achieved by exposing a substrate to appropriate precursors (typically gas molecules) in the presence of energy (thermal or plasma) in a reaction chamber. The precursors undergo reaction and/or decomposition on the surface of the substrate and form the desired solid thin film or powder. Any volatile by-products resulting in the process are removed by flowing gas through the chamber. In the context of supercapacitor devices and their fabrication, the CVD process is primarily used to synthesize carbon materials, including CNTs and nanofibers. Carbon film deposition by the CVD process generally employs precursor molecules such as acetylene, ethylene, carbon monoxide, and methane. The CVD method has been used to synthesize multi-walled carbon nanotubes (MWCNTs) and has been employed in flexible supercapacitor electrodes [58]. The sol–gel technique has been used to synthesize electrode materials for supercapacitors. Sol–gel, or solution gelling, is a method used to form solid thin films. In its essential form, the sol–gel method is achieved by dip coating a surface in a solution. Consequently, polymeric or particulate inorganic precursors are concentrated on a surface by a complicated process involving gravitational draining with simultaneous drying or solvent evaporation and continued condensation reactions, finally resulting in the formation of a solid film [59]. In a fundamental form, the chemical precipitation method involves the formation of a solid material from solution by means of a reaction. A solid substance is formed from a solution by one of two mechanisms: by the conversion of the substance into an insoluble form or by modifying the solvent composition to reduce the solubility of substance in it. This method has primarily been used in supercapacitor technology to synthesize electrode materials [60].

The microwave-assisted method has been employed to synthesize electrode materials for supercapacitors as an inexpensive, quick and versatile technique [61–64]. The microwave-hydrothermal (M-H) synthesis has inherent advantages, including good homogeneity, high yield, rapid volumetric heating, morphology controllability and the ability to produce narrow size distribution particles with high purity but it requires quite a long time to complete a reaction [24,65,66]. Incorporating rapid microwave heating into hydrothermal processing possesses a good potential for synthesizing inorganic materials, the M-H process is rapid and it improves the crystallization kinetics of synthesis process and thus M-H process is energy-efficient and economical [67].

In summary, microwave mediated synthesis method, due to microwave-induced accelerated kinetics, improved nucleation rate, and reduction in the reaction time, has drawn large attention in the synthesis of oxide materials for supercapacitors application [68]. The microwaves are non-ionizing electromagnetic radiations with a higher penetration depth, which leads to crystallites/particles with uniform dimensions and higher purity due to the absence of major thermal gradient in the reaction medium [66,68]. Table 4 summarizes the different electrode synthesis methods in terms of advantages, and disadvantages [38].

4. Metal oxides/hydroxides composite electrodes synthesized by microwave-assisted for supercapacitors

Generally, metal oxides can provide higher energy density for supercapacitors than conventional carbon materials and better electrochemical stability than polymer materials. They not only store energy like electrostatic carbon material but also exhibit electrochemical faradaic reactions between ions electrode and material within appropriate potential windows. In this review paper, the focus is on the development of a number of metal oxides/

Table 4
Different electrode synthesis methods (advantages and disadvantages) [28].

Synthesis methods	Advantages	Disadvantages
Electrochemical deposition method	Mass production; low costs; precise control on film thickness and uniformity	Process set up; current or voltage required
CBD	Simplicity; low temperature; inexpensive; large-area substrates	Limited flexibility; low material yield
CVD	High material yield than CBD; good film uniformity	Expensive equipment and relatively high costs
Sol–gel	Low costs; controllable film texture, composition, homogeneity, and structural properties	Complicated process
Chemical precipitation	Allows synthesis of composite electrode materials; efficient; easily implemented	May generate a waste product
Microwave-assisted	Facile; fast, quite; secure; controllable; energy-saving; decreasing synthesis time; an effective way to control particle size distribution and macroscopic morphology in the synthesis	Quite long time to complete a reaction

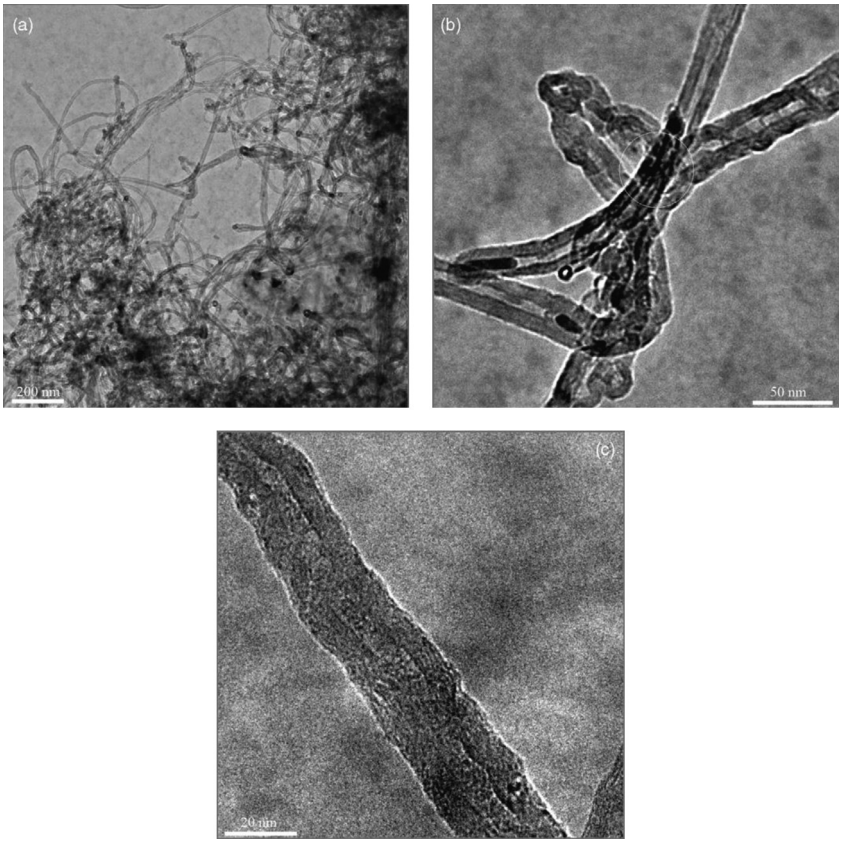

Fig. 8. TEM images of 20% RuO_2/MWCNTs [74].

hydroxides including ruthenium oxide, manganese oxide, nickel oxide, iron oxide, cobalt oxide, nickel hydroxide, cobalt hydroxide, nickel cobaltite, and etc. They have been examined for suitability as a supercapacitive material via a microwave-assisted technique.

4.1. Ruthenium oxide

Ruthenium oxides (RuO_2) have many advantages due to their stability, large-faradaic activity, and ion adsorption pseudocapacitance. Ruthenium-based supercapacitors, are not commercially viable because ruthenium is a low-earth abundant material and over 100 times more expensive than manganese and nickel starting reagents [69]. Carbon nanotubes (CNTs) have mainly been attractive as an electrode material for use in a supercapacitor due to the useful space within their cores and between neigh boring tubes, and good accessibility to their surfaces [70]. Therefore, many of studies have been made by hybridizing CNTs with RuO_2 as a composite for supercapacitor applications to exploit the advantages of these two individual components [71–73]. Yan et al. [74] reported the synthesis of RuO_2/MWCNTs nanocomposites through a simple, efficient and one-step microwave-assisted method, in which $RuCl_3$ solution as precursor and $NH_3 \cdot H_2O$ as precipitator. During the nanocomposites forming process, the chlorine ions could be easily removed because NH_4Cl decomposes at high temperatures [75]. The residual $NH_3 \cdot H_2O$ was also removed easily after microwave treatment. In addition, the intermediate product, $Ru(OH)_3$, changed directly into RuO_2 nanoparticles without extra annealing. It was found that RuO_2 nanoparticles could be attached to the side walls of MWCNTs. More importantly, some nanoparticles seemed to fill into the inner cavities of MWCNTs under the condition of microwave-assisted. RuO_2 nanoparticles was directly synthesized and attached onto MWCNTs in the mixture with $RuCl_3$ solution by microwave-assisted irradiation. Thus, significant enhancement in specific capacitance of RuO_2/MWCNTs composites has been prepared via microwave assisted method. TEM results demonstrate that RuO_2 nanoparticles have a narrow size distribution and are located on both inside and outside of MWCNTs through this preparation method (Fig. 8) [74]. Cyclic voltammetry results reveal that a specific capacitance of deposited RuO_2/MWCNTs electrode is considerably greater than other electrodes studied, mainly due to the contribution of RuO_2 nanoparticles. The content of RuO_2 in composite electrodes influences the capacitance. The MWCNTs/40% RuO_2 composite electrode is 493.9 F g^{-1} capacitances, higher than the MWCNTs/20% RuO_2 composite electrode with 232.5 F g^{-1}. Total resistance in MWCNTs, MWCNTs/20% RuO_2, and MWCNTs/40% RuO_2 are calculated to be 10.8, 9.48 and 7.31, respectively [74]. The as-prepared composites may have promising applications in high charge storage capacity devices, and etc.

4.2. Manganese oxide

Manganese oxides have different forms such as MnO_2, Mn_2O_3, Mn_3O_4, and MnO, due to their different oxidation states. Among the above mentioned structures, Mn_3O_4 is one of the most stable mixed oxides state ($Mn^{2+}(Mn^{3+})_2O_4$) and has the spinel structure. Mn_3O_4 is widely used in various fields such as electrode material for supercapacitor [76], anode material for lithium batteries [77], cathode material for fuel cells and metal-air batteries [78], and also used as an effective catalyst for the decomposition of waste gas. Therefore, it acts as a suitable material to control the air pollution [79].

Crystallized Manganese oxide (MnO_2) several crystalline structures, including α-, β-, γ-, and δ-MnO_2. Among them, α-, β-, and δ-MnO_2 have a tunnel structure (2 × 2 octahedral units for α-MnO_2,

the relatively large tunnel structured phase; 1 × 1 octahedral units for β-MnO_2, the more compact and dense phase), and δ-MnO_2 has a relatively open layered structure (as presented in Fig. 9 by Birnessite) [80]. It is well known that manganese oxides are considered as one of the most cost-effective transition metal oxides for the next generation of supercapacitors, due to their low cost, environmentally friendly nature, functional in neutral aqueous electrolytes and high theoretical specific capacitance. Manganese oxide is also regarded as a replacement for RuO_2 in a supercapacitor. Unfortunately, the use of MnO_2 usually produces a low specific capacitance, due to its poor electrical conductivity and lack of accessible surface area [81]. MnO_2 has been taken into intensive investigations because of its superior electrochemical performance that depends on various factors, such as structure, particle size, surface morphology, homogeneity and bulk density. These factors can influence kinetics of H^+ or alkali metal cations (C^+) diffusing process, the adsorbability, and utilization ratio of MnO_2 [82]. Different syntheses of MnO_2 make crystal growth environments vary, and thus leading to different physical and chemical properties, such as crystallinity, morphology, specific surface (SS) area and cycling stability [81,83]. A literature survey shows that many routes or techniques for preparation of MnO_2 have been developed. Previous approaches to the synthesis of MnO_2/carbon included various methods such as physical mixing [84], thermal decomposition [85–87], electrodeposition [55,88,89], sol–gel [59,90], redox reactions [8,84] and microwave-assisted synthesis [24,91–93]. Most of the methods require extensive mechanical mixing, long duration, high temperature, energy-wasting, etc. In recent years, microwave-assisted synthesis of inorganic materials has received a great attention as it can shorten the reaction time from several hours to a few minutes with enormous energy savings [61–64]. Thus, microwave heating has been introduced to assist in the synthesis of MnO_2 [94–98]. For example, Nyutu et al. [97] prepared α-MnO_2 nanofibers in mixed aqueous and dimethyl sulfoxide solvent by using microwave reflux. This process required about 10 min to start crystallizing the α-MnO_2 phase and about 90 min to fully crystallize the phase. Huang et al. [98] used a microwave hydrothermal technique to prepare α-MnO_2 nanofibers at 200 °C with a hold time of 10 s–30 min. Meher and Rao [91] demonstrated better surface properties like uniform surface morphology, high surface area, pore volume and bimodal pore size distribution of α-MnO_2 samples synthesized under microwave assisted method as compared to conventional-reflux methods. Ming et al. [24] reported the synthesis of γ-MnO_2 nanospheres by microwave hydrothermal method at 75 °C for 30 min. A facile process to synthesize MnO_2 with different crystal structures and morphologies is still a challenge by microwave-assisted method. γ-MnO_2 nanoparticles and α-MnO_2 urchin-like nanostructures have been successfully synthesized by microwave-assisted reflux as short as 5 min under neutral and acidic conditions, respectively [99]. Chen et al. [100] reported a coupled microwave-hydrothermal process to crystallize polymorphs of MnO_2 such as α-, β-, and γ-phase samples with plate-, rod-, and wire-like shapes, by a controllable redox reaction in $MnCl_2$–$KMnO_4$ aqueous solution system. Microwave-assisted method is facile but it is easy to go to thermal runway [82], and the hydrothermal synthesis is beneficial for making smaller particles but it requires quite a long time to complete a reaction [101]. The process combines the advantages of hydrothermal and microwave-assisted synthesis. A literature survey reveals that few reports about M-H synthesis of MnO_2 as electrode materials can be found. The Bir-MnO_2 nanospheres have been synthesized by M-H method at 75 °C for 30 min under very low pressure. It exhibits a large SS of 213.6 $m^2\ g^{-1}$. The electrochemical test results show that the Cs is 210 F g^{-1} at 200 mA g^{-1} in 1.0 M Na_2SO_4 electrolyte. Cs retention and coulombic efficiency are over 96% and 98%, respectively after 300 cycles at 1.6 A g^{-1}.

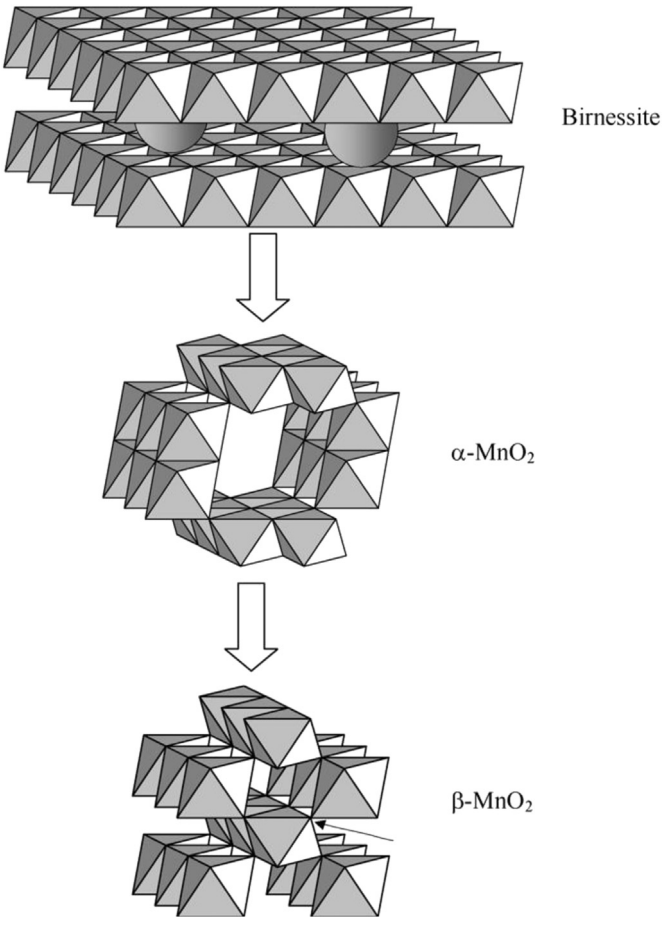

Fig. 9. Manganese dioxide structural transitions induced during material synthesis [80].

Interestingly, CNT/MnO_2 composites that have been prepared by microwave irradiation, are very suitable and promising electrode materials for supercapacitors with high power and energy densities [93,102]. Aligned carbon nanotube (ACNT)/MnO_2 nanocomposites are fabricated using the reduction between potassium permanganate and ACNT under microwave irradiation as shown in Fig. 10 [102]. Nanoscale MnO_2 particles were uniformly deposited on the surface of compressible spring-like ACNTs, which recover themselves during the charge/discharge process to maintain good contact with current collector, due to their excellent mechanical strength and compressibility. The morphology of ACNTs presents a stacking structure with a length of 5–20 μm as presented in Fig. 11(a). After MnO_2 deposition, the stacking structure of ACNTs still keeps its morphology (Fig. 11(b and c)). The self-limiting reaction between permanganate and carbon was applied to deposit birnessite MnO_2 onto the surface of ACNT (the diameter of 10–20 nm, Fig. 11(d)). Therefore, the advantage of this process is that thin MnO_2 film is closely anchored to the surface of nanotubes (Fig. 11(e)). For comparison, pure MnO_2 with flower-like structure was also prepared by hydrothermal synthesis method (Fig. 11(f)). The stacking structure of ACNT also improves the diffusion of electrolyte ions in the electrode and promises a high-rate electrode material for supercapacitor [102]. Therefore, a high specific capacitance and good rate capability of MnO_2 can be achieved [102,103]. For CNT–15%MnO_2 composite, the specific capacitance based on MnO_2 is 944 (85% of the theoretical capacitance) and 522 F g^{-1} at 1 and 500 mV s^{-1}, respectively. When the content of MnO_2 reaches

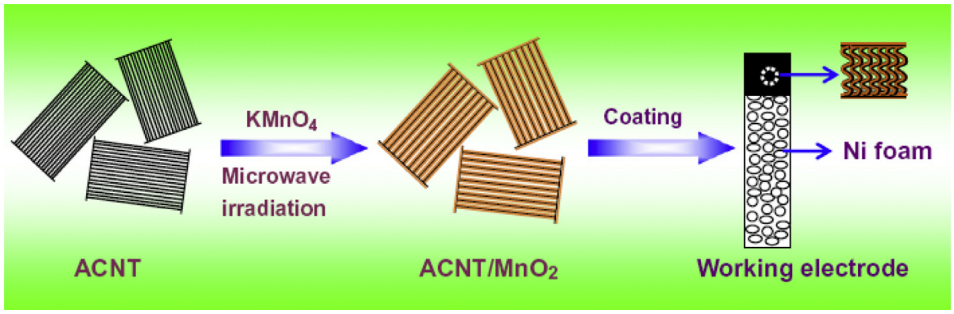

Fig. 10. Schematic illustration of the synthesis of ACNT/MnO_2 composite as electrode material [102].

57 wt.%, the composites have the maximum power density (45.4 kW kg^{-1}, the energy density is 25.2 Wh kg^{-1}) [93]. Therefore, CNT/MnO_2 composites prepared by microwave irradiation are promising electrode materials in hybrid vehicle systems.

Consequently, the addition of CNTs such as single-walled CNTs (SWCNTs) [104], multi-walled CNTs (MWCNTs) [103] into MnO_2 is expected to not only significantly improve the electronic conductivity but also provide better mechanical robustness for the composite. Double-walled carbon nanotubes (DWCNTs)/δ-MnO_2 composites have been synthesized by the reduction of potassium permanganate under microwave irradiation [105]. The mass loading of MnO_2 on carbon can reach as high as 85%, which is the highest content as reported in literature [105]. Graphene based materials coupled with transition metal oxides are promising electrodes in asymmetric supercapacitors, owing to their unique properties which include high surface area, good chemical stability,

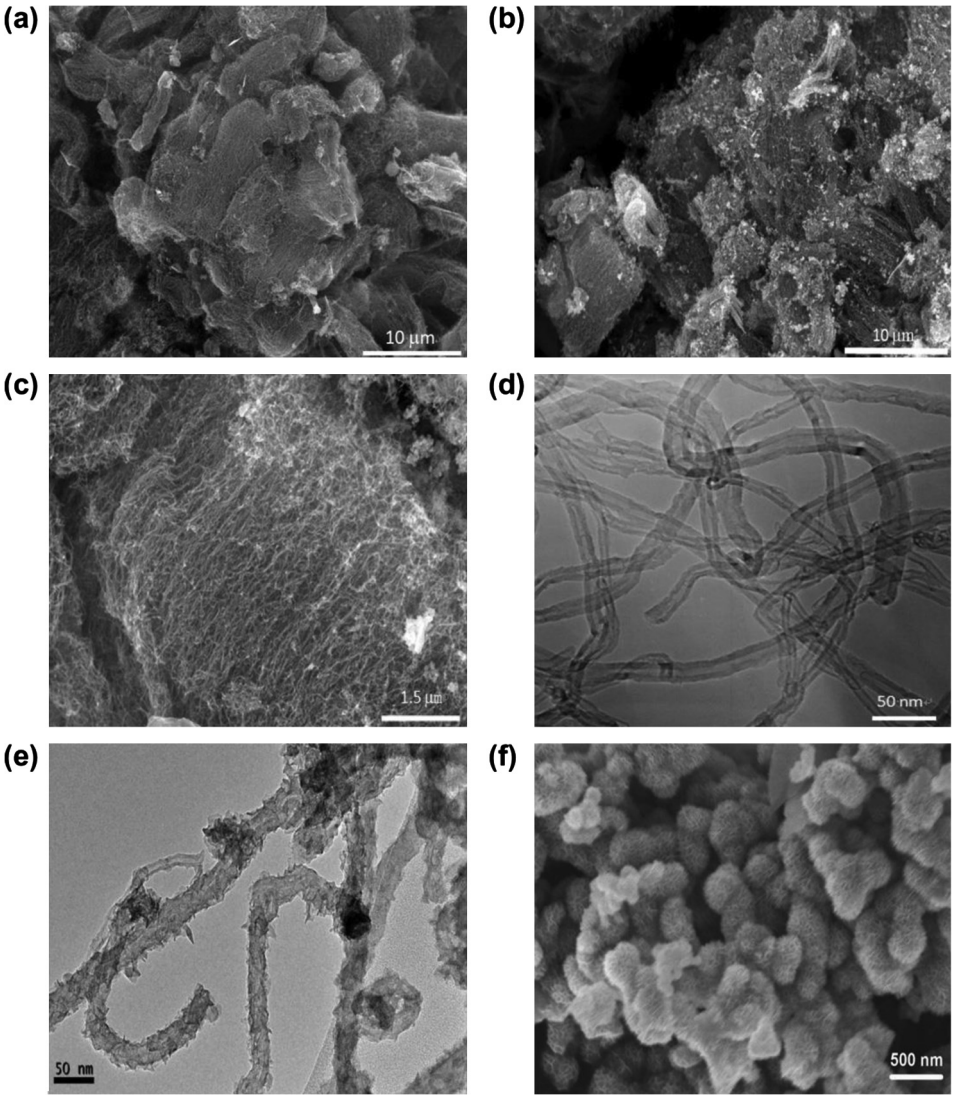

Fig. 11. SEM images of ACNT (a) and ACNT/48%-MnO_2 (b and c). TEM image of ACNT (d) and ACNT/48%-MnO_2 (e). SEM image of pure MnO_2 exhibiting flower-like structure (f) [102].

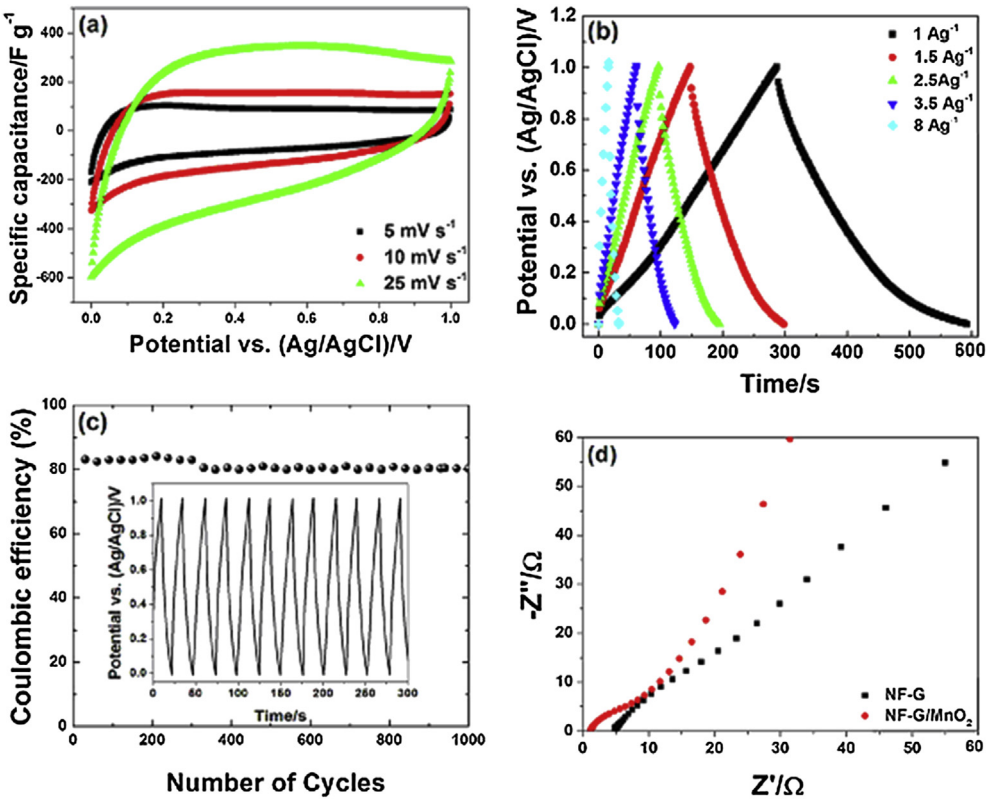

Fig. 12. Electrochemical results for NF–G/MnO_2 composite. (a) Cyclic voltammetry curves of NF–G/MnO_2 composite measured at different scan rates. (b) The galvanostatic charge–discharge curve at different current densities. (c) The coulombic efficiency of the composite at a current density of 2.5 A g^{-1} (the inset to the figure shows the continuous charge–discharge curve) and (d) EIS plot of both NF–G and NF–G/MnO_2 [95].

electrical conductivity, abundance, and lower cost profile over time. Some works on graphene-MnO_2 (GN/MnO_2) composites have been reported [100,106,107]. Yang et al. [106] and Yan et al. [107] studied supercapacitor electrodes based on GN/MnO_2 composite materials, which were synthesized by different methods, and observed good electrochemical performance. Different morphologies of manganese dioxide may have a dramatic influence on capacitance. Thus, a large enhancement of the capacitance may be obtained by using graphene and different morphologies of MnO_2 composite materials. Chen et al. [100] reported a rapid and easy method for preparing GN/MnO_2 composites as electrode materials, which included adding $MnSO_4 \cdot H_2O$ solution to a well-dispersed graphene liquid and then adding $KMnO_4$ solution; microwave-assisted synthesis was applied to the mixture solution at 75 °C for 30 min. Hierarchy structure composites had better contact with each other than single form ones. The composites were prepared as supercapacitor electrodes, and the experimental results showed that the electrodes exhibit good specific capacitance in 1 mol L^{-1} Li_2SO_4 and good cyclic stability [100].

A composite material consisting of graphene oxide exfoliated with microwave radiation (mw rGO), and manganosite (MnO) has been synthesized in order to explore their potential as an electrode material. The best composite electrode containing 90% MnO–10% mw rGO (w/w) exhibits a capacitance of 0.11 F cm^{-2} (51.5 F g^{-1} by mass) and excellent capacity retention of 82% after 15,000 cycles at a current density of 0.5 A g^{-1} [63].

Spherical Mn_3O_4 nanoparticles have been synthesized by microwave assisted reflux method at different reaction times (1, 5, 10, 15, and 20 min) [108]. Liu et al. [65] has been synthesized crystalline hausmannite nanocrystals/reduced graphene oxide composites (denoted as Mn_3O_4/RGO) by means of microwave-assisted hydrothermal synthesis (MAHS) route for the application of symmetric and asymmetric supercapacitors with specific capacitance (~193 F g^{-1}). The device energy and power densities show 11.11 Wh kg^{-1} and 23.5 kW kg^{-1} values, respectively.

A green chemistry approach (hydrothermal microwave irradiation) has been used to deposit manganese oxide on nickel foam–graphene (NF–G). The 3D graphene was synthesized using nickel foam template by chemical vapour deposition (CVD) technique. Meanwhile, the results show that pseudocapacitance can be effectively loaded onto the surface of NF–G via microwave irradiation and has the potential for high performance supercapacitor application. Electrochemical results for NF–G/MnO_2 composite are shown in Fig. 12(a)–(d) [95]. Fig. 12(a) presents the NF–G/MnO_2 CV curves at different scan rates, showing a relatively rectangular shape, which is a characteristic of an ideal capacitive behaviour. This figure also indicates that the composite electrodes exhibit good electrochemical reversibility between 0 and 1 V. Fig. 12(b) illustrates the discharge curve of NF–G at a current density of 1 A g^{-1}. The curve displays a non-linear behaviour, indicating a pseudocapacitive effect. Fig. 12(c) reveals that the galvanostatic cycling performance of the composite has been established to be stable, with cycle efficiency (Coulombic efficiency) of about 80% for 1000 charge/discharge cycles, which reveals the excellent stability and performance of the electrode. The EIS (Nyquist) plot of NF–G and NF–G/MnO_2 is shown in Fig. 12(d). It is an illustration of the real and imaginary part of the impedance of the electrode material. It is worth stating that for ideal supercapacitors, the Nyquist plot should be a line perpendicular to the real axis at low frequency. The Nyquist plot of NF–G/MnO_2 shows that it is much closer to the ideal behaviour which might be attributed to the low charge transfer of G and MnO_2; thus demonstrating a better capacitive behaviour [95].

4.3. Iron oxide

Iron (Fe) is an important earth-abundant chemical element. It commonly exists as +2 and +3 oxidation states in solution. The common iron–oxygen compounds are Fe_2O_3, FeOOH, Fe_3O_4 and FeO. Fe-based compounds can be synthesized by controlling the valence state of the soluble iron salts of Fe^{3+} and Fe^{2+} ions in solid or solution phases. For example, Mn-based compounds of different phases, structures and sizes have been formed by controlling the chemical reactions of Mn^{2+} and Mn^{7+} [109]. The chemical-reaction-controlled synthesis is a promising and powerful route to crystallize nano/micro transition metal oxide [110,111]. Iron oxides are potential electrodes as in lithium-ion batteries and supercapacitors owing to their low cost and low toxicity [112]. Various synthesis methods have been used to grow iron oxides with different structures, phases, sizes, and their electrochemical performances have been evaluated as electrode material. The microwave-hydrothermal process is potentially advantageous for the synthesis of iron oxide. Herein, was port the synthesis of Fe-based oxide materials of Fe_2O_3, Fe_3O_4, and FeOOH by the microwave-hydrothermal process, using short reaction times (15 min to 2 h). Cube-like Fe_2O_3, FeOOH nanorods and Fe_3O_4 particles were crystallized by the controllable hydrolysis and redox reactions of $FeCl_3$ or $FeCl_2$. The Fe based materials were processed to make anodes and cathodes of lithium-ion battery and supercapacitor to study their potential electrochemical applications. The electrochemical measurement results showed that FeOOH had a better anodic capacity as lithium-ion battery than that of either Fe_2O_3 or Fe_3O_4. Also the microwave-hydrothermally synthesized Fe-based materials were investigated as promising lithium-ion battery anode and supercapacitor materials [113].

4.4. Nickel oxide/hydroxide

Nickel oxide (NiO) with high-specific surface area and high porosity, is one of the materials suitable for pseudocapacitor electrode applications, owing to its high theoretical specific capacitance, low cost, high chemical, and thermal stability [62]. The electrochemical performance of NiO nanostructures is strongly influenced by its morphology. NiO with a high theoretical capacitance value of 2573 F g^{-1}, a distinct redox reaction, and a controllable morphology has become a popular pseudocapacitive material for supercapacitors [114–116]. NiO, as an electrode material for supercapacitors, has been reported in the form of nanoflakes [117], quasi-nanotubes [118], nano/microspheres [119], and nanosheet hollow spheres [120]. Among these, nanoflakes have several advantages in supercapacitor applications. Nanoflakes enhance the diffusion of electrolyte and provide more paths for diffusion of ions leading to improvement in the performance of the electrode [121]. NiO nanoflakes were synthesized by various methods such as precipitation [117], and hydrothermal method [122], but microwave assisted heating is an easy route of obtaining these morphologies. Microwave heating increases the reaction kinetics that induce the quick formation of nanoflakes by oriented attachment [123]. Microwave chemistry is based on effective heating of material rather than inducing chemical reactions of electromagnetic radiation. This heating mechanism includes dipolar polarization and ionic conduction [68]. Obermayer et al. [124] confirmed the enhancement of growth kinetics in microwave assisted synthesis to be purely due to temperature effect and not due to the influence of electromagnetic reaction. There are numerous reports on the synthesis of NiO with different nanostructured configurations and morphologies via microwave method for possible use in supercapacitor applications. For example, NiO nanoflowers synthesized by microwave method at 15 min of microwave heating exhibit maximum specific capacitance of 277 F g^{-1} at scan rate of 2.5 mV s^{-1} [125]. Cao et al. [126] reported maximum specific capacitance of 770 F g^{-1} at discharge current of 2 A g^{-1} for flower-like NiO hollow nanosphere synthesized, using the gas/liquid interface via a microwave method at 170 °C in 3 min of microwave treatment and heat treatment of particles at 170 °C for 30 min. Meher et al. [127] reported the synthesis of porous ball like NiO by nonhydrothermal microwave-reflux at 120 °C for 15 min. It was reported to exhibit maximum specific capacitance of 420 F g^{-1} at 0.5 A g^{-1}. Vijayakumar et al. [128] reported a 5 min synthesis of NiO nanoflakes using the microwave method using cetyltrimethyl ammonium bromide (CTAB) as a surfactant. Time evolution study has been performed, and a possible mechanism of formation of nanoflake structured NiO has been proposed in a pictorial manner. The electrochemical performance of NiO nanostructures, prepared via a microwave-assisted method and calcination at 300, 400, and 500 °C, as a supercapacitor electrode material in 2.0 M KOH electrolyte, has been reported and discussed. Behm et al. [62] synthesized a NiO-nanoplate–SWCNT composite film by employing homogeneous precipitation method under microwave-reflux and conventional-reflux conditions. The aim was to bring out the physicochemical and pseudocapacitive distinctiveness of NiO sample prepared by nonhydrothermal microwave-reflux method, as compared to conventional-reflux method. The composite was tested and showed enhanced pseudocapacitance behaviour. Further optimization of the SWCNT chirality, metal percent composition, and abundance *vs.* NiO yields significantly higher capacitances, power densities, and higher operating voltages.

Due to their small sizes, nanoparticles exhibit novel material properties that are significantly different from their bulk counterparts. Nickel hydroxide ($Ni(OH)_2$), as one of the most important transition metal hydroxides, has received increasing attention due to its extensive applications as an active material in the power tools, portable electronics, electric vehicles, and positive electrodes [129,130]. There are two polymorphs of $Ni(OH)_2$, which are designated as α-$Ni(OH)_2$ and β-$Ni(OH)_2$. The α-$Ni(OH)_2$ phase is relatively disordered with larger interlayer spacing (>7.5 Å), which can place higher amounts of anions like nitrate, carbonate, sulphate as well as water molecules. The hexagonal β-$Ni(OH)_2$ phase is brucite-like with well-oriented $Ni(OH)_2$ layers which are perfectly stacked along the c-axis with an inter lamellar distance of about 4.60 Å [131–134]. Owing to the high tap density and excellent electrochemical activity, spherical β-$Ni(OH)_2$ has been used as an active material with large-scale production for the contemporary alkaline Ni-based batteries. The performance of $Ni(OH)_2$ depends on its size, morphology, and structural characteristics [135–137]. In recent years, rapid progress has been made in the preparation of $Ni(OH)_2$ nanoparticles with desired size and shape, as well as the various nanostructures such as nanorods [138], nanotubes [135,136], nanosheets [139–141], stacks of pancakes [131], hollow spheres [142,143], and carnation-like structures [144]. Nickel oxy-hydroxide, $Ni^{III}OOH$, can be prepared by oxidation of $Ni^{II}(OH)_2$ precursor without significant symmetry change (a = 2.8 Å, c = 4.7 Å), but with a broadening of the diffraction peaks, as revealed by XRD investigations [145,146]. NiOOH products prepared from Al-substituted spherical α-$Ni(OH)_2$ or Co coated spherical β-$Ni(OH)_2$ precursors were reported elsewhere [147,148]. The different nickel hydroxides and oxy-hydroxides crystallographic phases are described by a layer type structure built up of a packing along the c-axis, of brucite type slabs made of edge-sharing NiO_6 octahedra [145,146]. Structural information about α and γ (oxy)hydroxides have been investigated [145]. The (II)/(III) redox reaction can be formally written as:

$$Ni^{II}(OH)_2 \leftrightarrow Ni^{III}O(OH) + H^+ + e^- \quad (11)$$

$Ni(OH)_2$ is cost effective and available in various morphologies, making it an attractive candidate for high performance supercapacitors [149,150]. In attempts to improve the electrochemical performance of $Ni(OH)_2$-based electrodes, $Ni(OH)_2$ nanostructures have been studied, [130,151] as well as $Ni(OH)_2$–carbon composites involving high surface area conductive materials such as activated carbon [152,153], carbon nanotubes, [154,155] and graphene [156–159]. These materials can improve the conductivity of the composites and shorten the electron and ion diffusion pathways with the aim of more efficient charge and mass exchange. Such nanostructured composites have always been coated to a metal current collector to obtain a continuous conductive structure, which greatly decreases the overall gravimetric specific capacitance.

Hierarchical flowerlike nickel hydroxide decorated on graphene sheets was prepared by a facile and cost-effective microwave-assisted method. In order to achieve high energy and power densities, a high-voltage asymmetric supercapacitor was successfully fabricated using $Ni(OH)_2$/graphene and porous graphene as the positive and negative electrodes, respectively. Because of their unique structure, both materials exhibit excellent electrochemical performance. The optimized asymmetric supercapacitor can be cycled reversibly in the high-voltage region of 0–1.6 V and displays intriguing performances with a maximum specific capacitance of 218.4 F g^{-1} and high energy density of 77.8 Wh kg^{-1}. In addition, the $Ni(OH)_2$/graphene//porous graphene supercapacitor device exhibits excellent long cycle life along with 94.3% specific capacitance retained after 3000 cycles [160].

It was also as reported a facile and large-scale production strategy for the synthesis of the mesoporous α-$Ni(OH)_2$ material via the homogenous hydrolysis of hexamethylenetetramine and nickel nitrate in ethylene glycol solution, assisted with microwave heating. The obtained α-$Ni(OH)_2$ was used as a precursor for preparing nickel oxides (NiO_x) through a simple annealing treatment at 250 °C for 3 h. NiO_x has similar morphology to its precursor α-$Ni(OH)_2$, which is nanoball-like with large surface area. It was found that an electrode based on NiO_x in alkaline solution could display excellent electrochemical behaviour with a specific capacitance of 650 F g^{-1} at 20 mV s^{-1} and still maintained 92% of its maximum specific capacitance after 1000 charging–discharging cycles [161].

4.5. Cobalt oxide/hydroxide

Among the transition metal oxides, cobalt oxide has three well-known polymorphs; monoxide or cobaltous oxide (CoO), cobaltic oxide (Co_2O_3) and cobaltosic oxide or cobalt cobaltite (Co_3O_4). CoO is the final product formed when the cobalt compound or other oxides are annealed at a sufficiently high temperature (1173 K) [162]. Pure CoO is difficult to obtain, since it readily takes up oxygen even at room temperature to reform to a higher oxide [163]. Cobaltic oxide (Co_2O_3) could be formed when cobalt compounds are heated at a low temperature in the presence of excess air. Some authors have reported that Co_2O_3 exists only in the hydrated form [164]. Co_2O_3 completely converted into Co_3O_4 at 538 K. Co_2O_3 absorbed oxygen in sufficient quantity and transforms to a higher oxide Co_3O_4, with no change in the lattice structure [165]. Cobalt oxide is one of the most studied oxides, due to its appealing multifunctional properties. Nanostructured Co_3O_4, the most stable cobalt oxide with a spinel-type structure comprising of both Co(II) and Co(III), is an important p-type semiconductor for many industrial applications in the area of secondary Li/O_2 cells as negative electrodes for Li-ion batteries [166] as well as in the field of emitters [167], heterogeneous catalysts [168,169], electrochemical capacitors for high power devices in energy systems, electrochromic devices, solar selective absorbers, solid-state sensors [170], protective layers or pigment for glasses and ceramics [2], superhydrophobic surfaces [164], and supercapacitors [171]. On the other hand, less studies have been focused on cobalt monoxide (CoO) nanostructures, which are hard to synthesize because of the special requirements necessary to force cobalt in a low oxidation state under common ambient conditions [171]. Cobalt oxide is reported to be a promising electrode material for supercapacitors because of its relatively low cost, high redox activity, high theoretical specific capacitance (~3560 F g^{-1}) and its great reversibility [172]. Among the most active transition metals, Co_3O_4, due to its high surface area, good redox and easily tuneable surface, as well as structural properties, has been studied extensively for supercapacitor applications [22,173]. Co_3O_4 is equally important in heterogeneous catalysis [174,175], solid state sensors [176,177], and magnetic materials [178]. Mainly, one-dimensional Co_3O_4 nanowire is fascinating for its widespread applications due to the reduced particle size and higher surface area, thus generating larger active interfacial sites [179]. Consequently, the synthesis of one-dimensional Co_3O_4 nanostructures by using porous alumina or virus as templates [180], thermal conversion of cobalt hydroxide nanostructures using hydrothermal route [181], electrochemical deposition [182], and many other methods [183] is widely studied and explored for numerous applications. The use of porous alumina or virus as template is, quite intricate and costly. The use of the hydrothermal method is widely accepted due to easily controllable parameters; however, the control of the shape of the nanoscale particles emerging from a hydrothermal process is quite tricky, due to the possibility of formation of added secondary products [184]. Therefore, the synthesis of Co_3O_4 nanowire using a facile and nonhydrothermal method is still a reasonable challenge. The microwave-mediated synthesis was adopted to prepare Co_3O_4 with regular microstructures [21,173]. Most of the reported synthesis methods are hydrothermal-mediated, where the effect of the hydrothermal condition confines the clear understanding of microwave effect on the morphology of Co_3O_4. Therefore, synthesis of Co_3O_4 by a nonhydrothermal microwave method has been essential to understand the effect of microwave on the crystallinity, morphology, and other properties of the material. In this case, Meher and Rao [185] synthesized the Co_3O_4 sample by the conventional reflux method, consisting of randomly distributed thin nanowires, while the microwave reflux method generates higher-dimensional and arranged Co_3O_4 nanowires. The surface area and pore structural analysis of the Co_3O_4 samples showed significant difference in their meso- and macroporosity, as well as specific surface area, due to differently crystallized products.

Cobalt hydroxides, $Co(OH)_2$ and $Co(OH)_2$-based materials are known as inexpensive, nontoxic and electrochemically active redox materials. They are attractive due to their layered structure and large interlayer spacing, which promises high surface area and a fast ion insertion/desertion rate. Some publications exist on $Co(OH)_2$-based materials for ES [61,186–188]. For example, Kong et al. [189] showed a pseudocapacitive behaviour of the $Co(OH)_2$ nanoflakes. Hu et al. [190] showed that the specific capacitance of sheet-like $Co(OH)_2$ is about 416.7 F g^{-1}. Gupta et al. [191] have shown a high specific capacity of cobalt hydroxide nanomaterial deposited electrochemically on a stainless steel electrode. Zhou et al. [192] reported a very high specific capacitance (1084 F g^{-1}) of mesoporous $Co(OH)_2$ film deposited electrochemically on a titanium substrate. Although a high specific capacitance was achieved using electrochemical methods, a poor yield of electroactive material is the main drawback of these methods. Therefore, preparation of $Co(OH)_2$ in gram scale, having high specific capacitance is a burning problem for researchers.

Crystalline Co_3O_4 and $Co(OH)_2$ have been synthesized using $Co(NO_3)_2$ as a precursor by conventional-hydrothermal and

microwave-hydrothermal routes, respectively. The Co_3O_4 phase shows cubic morphologies (Fig. 13(a)) while the β-$Co(OH)_2$ phase exhibits plate-like shapes (Fig. 13(b)). The electrochemical performances of Co_3O_4 and $Co(OH)_2$ phases are evaluated as electrode materials for lithium-ion battery anodes, cathodes and supercapacitors. Both Co_3O_4 and $Co(OH)_2$ phases show pseudocapacitive performances in Li_2SO_4 and KOH electrolytes. The Co_3O_4 and $Co(OH)_2$ phases are found to be more promising as anodes than as cathodes in lithium-ion batteries. $Co(OH)_2$ electrodes show higher specific capacitances than those of Co_3O_4 materials. The capacity of Co_3O_4 anode for lithium-ion battery is 168.1 mAh g^{-1}, after 50th discharge–charge cycle. The specific capacitance of $Co(OH)_2$ supercapacitor in KOH electrolyte is 64 F g^{-1} [193].

4.6. Tungsten oxide

Tungsten oxides (WO_3) in both crystalline and amorphous forms are widely studied as an electrode material for sensors [194] and electrochromic devices [195]. Unfortunately, the electrochemical properties of both amorphous and crystalline WO_3 are not suitable for the application of ECs because of the limited potential window as well as the relatively poor reversibility of proton and Li ion intercalation/de-intercalation [196]. Consequently, tungsten oxides of certain microstructures should be of pseudocapacitive behaviour [197–200]. One order of magnitude improvement in specific capacitance is achieved with the present composition, from 54 F g^{-1} for WO_3 nanoparticles to 700 F g^{-1} for WO_3/CA composites (scanned at 25 mV s^{-1} in 0.5 M H_2SO_4 over a potential window of −0.3 to 0.5 V) [197]. Since the potential window for the reversible intercalation/de-intercalation of protons within tungsten oxides is in the UPD (under potential deposition) and OPD (over potential deposition) hydrogen regions [201], meanwhile concentrated acidic solutions are suitable electrolytes for the redox transitions of tungsten oxides [202], a tungsten oxide anode and a RuO_2 cathode was proposed to construct an asymmetric EC with a wide working voltage to advance the energy density of ECs by many chemical routes, such as precipitation method [203], electrochemical deposition [204] hydrothermal synthesis [205,206] were developed to prepare tungsten oxides. Tungsten oxides in both crystalline and amorphous forms prepared by these methods commonly show unacceptable performances for the EC application.

Hence, microwave irradiation was considered as a promising method. Huang et al. [195] synthesized tungsten oxide by microwave, which was used for the first time as material for supercapacitor electrode with specific capacitance 231 F cm^{-2}. Chang et al. [207] synthesized tungsten oxides by microwave-assisted hydrothermal (MAH) process with high-rate capability for ECs. Jeong and Manthiram [208] reported that RuO_2 coated with WO_3 shows good capacitive performance in both acidic and alkaline media in 2001. Finally in 2011, a tungsten oxide anode and a RuO_2 cathode were proposed to construct an asymmetric EC with a wide working voltage to advance the energy density of ECs [207].

Crystalline tungsten oxide mixtures, WO_3–$WO_3 \cdot 0.5H_2O$, prepared by microwave-assisted hydrothermal that shows capacitive-like behaviour at 200 mV s^{-1} and specific capacitance 290 F g^{-1} at 25 mV s^{-1} in 0.5 M H_2SO_4 between −0.6 and 0.2 V [49].

4.7. Tin oxide

Pseudo-capacitive materials generally low conductivity and pseudocapacitors solely based on them cannot support fast electron transport required at high rate. In such hybrid material where these pseudo-capacitive materials are decorated on the continuous graphene network. Highly conductive graphene network ensures fast electron transport through the supercapacitor electrode and improvement can be expected with the introduction of pseudocapacitance. For example, Niu et al. [70] synthesized graphene/tin oxide (G/SnO_2) nano-composite in acid solution, achieving higher specific capacitance compared to graphene and graphene oxide. Wang et al. [209] developed a novel one-pot synthesis strategy to prepare both SnO_2/graphene nanocomposites and PtRu/graphene with the microwave-assisted polyol process for their electrochemical performance. The synthesis approach was effective and fast, since the microwave heating provided sufficient heat needed for the reaction within very short time and the reduction of graphene oxide (GO) to graphene (G) and the conversion of SnO_2 nanoparticles from $SnCl_2$ precursors and the reduction of PtRu nanoparticles from their metal precursors are realized simultaneously in this one-pot approach. The specific capacitance of microwave SnO_2/G and G is 99.7 F g^{-1} and 52.7 F g^{-1}, respectively. The enhanced specific capacitance of SnO_2/G electrode is related to the pseudocapacitance that originates from the uniformly distributed tin oxide nanoparticles on graphene [209].

The electrochemical investigation for supercapacitor and fuel cell application indicates that the as-prepared electrode materials shows advantageous performance, which could be attributed to the good dispersion of metal or metal oxide nanoparticles on graphene and their synergetic interaction with grapheme support.

4.8. Zinc oxide

Zinc oxide (ZnO) exhibits excellent optical and electrical properties and hence they have been widely used in solar cells, gas censors and short-wavelength light-emitting devices [11]. Also, ZnO is known to be a battery active material, having high energy density of 650 A g^{-1}, received special attention as electrode

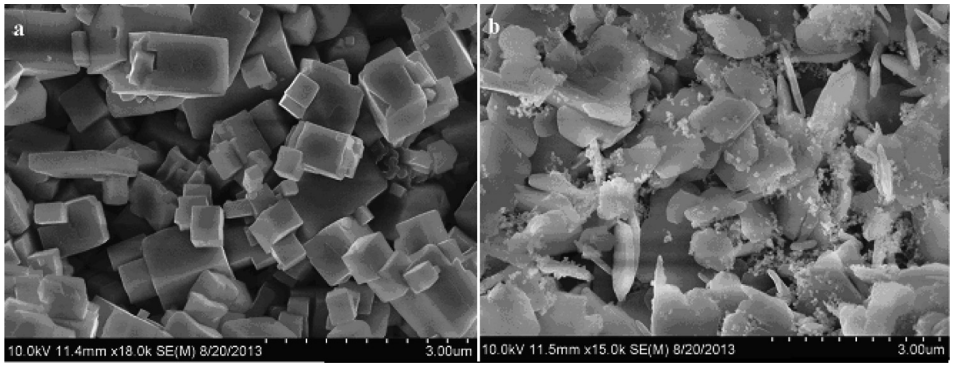

Fig. 13. SEM images of as-obtained Co-based products. (a) Co_3O_4 obtained by conventional-hydrothermal treatment of $Co(NO_3)_2$ at 200 °C for 5d, and (b) $Co(OH)_2$ obtained by microwave-hydrothermal treatment of $Co(NO_3)_2$ at 140 °C for 2 h [193].

material [12]. But it has the disadvantage of formation of dendrite growth during consecutive cycling, which leads to decrease in cycle life. Because of its good electrochemical activity and eco-friendly nature, zinc oxide can be a promising electrode material for supercapacitor [210,211]. Various methods like ultrasonic spray pyrolysis (USP) [212,213], microwave assisted synthesis [214], mechanical mixing [215] and green synthesis [216] were employed for the preparation of ZnO/carbon composite electrode for achieving high performance supercapacitor. These methods are multi-step wet processes in which, carried over residual impurities might affect electrochemical properties. These electrodes are shown to have limited improvements in the supercapacitor performance. Hence it is important to develop facile and dry processes to modify electrodes that will show better results in the electrode performance. Ouldhamadouche et al. [217] and Tan et al. [218] used sputtering technique for coating ZnO on vertically aligned carbon nanotube. These composites were used for photoluminescence applications. For the first time, Aravinda et al. [219] reported a binder free method for the preparation of ZnO/carbon nanotube composite for supercapacitor electrodes, using magnetron sputtering of ZnO over FWNTs. The capacitance of FWNTs electrode is significantly increased from 33 F g^{-1} to 59 F g^{-1}.

ZnO/C composite has been synthesized by self-propagating solution combustion method using dextrose as fuel and carbon source. By this method, carbon is added in-situ to the metal oxide and shows an electrochemical capacitance of 21.7 F g^{-1} [211]. Fig. 14 [211] reveals the SEM image of ZnO/C composite; the particles are agglomerated and their sizes lie in the range of 35–85 nm. While nanostructured ZnO has been prepared by a facile microwave method and used to prepare electrodes by compositing with AC [215]. The FESEM image of the ZnO samples (Fig. 15(a)) indicates a wide distribution of particle sizes ranging from 10 to 200 nm and exhibits only irregular granular feature. Fig. 15(b) illustrates the SEM image of nano ZnO-AC carbon composite. The image clearly shows the coating of the nanostructured ZnO on to AC. This kind of surface morphology is quite ideal for the fabrication of the electrode as it would be having high surface area and expected to yield a specific capacitance of 160 F g^{-1} for 1:1 composition [215].

Considering the excellent properties of graphene and ZnO, a combination of graphene with ZnO nanoparticles (NPs) might give enhanced performance in supercapacitors [220,221]. Lu et al. [214] carried out one-step synthesis of graphene–ZnO nanocomposite through microwave-assisted reduction of zinc ions in aqueous solution with GO dispersion using a microwave synthesis system. The electrochemical tests show that graphene–ZnO composite exhibits an improved electrochemical capacitance of 146 F g^{-1} with good reversible charge/discharge behaviour.

4.9. Copper oxide

Copper oxides in forms CuO and Cu_2O have been widely used as catalysts, gas sensors, adsorbents, and electrode materials. The different morphologies of CuO have attracted more interest for practical application. Compared with nanoparticles, CuO whiskers are expected to exhibit remarkable optical, electrical, magnetic, and mechanical properties. In electrochemical field, few reports have been exhibited the application of cupric (cuprous) oxides as electrode materials on batteries [222,223]. Bijani et al. [222] prepared Cu_2O thin film electrodes by electrodeposition, for lithium batteries and the films could provide a specific capacitance of 350 Ah kg^{-1}. Wang et al. [223] reported the application of CuO film prepared by solution immersion on lithium batteries, and the thin film with network-like structure as negative electrode exhibited a capacity of 560 mAh g^{-1} and long cycling life. Zhang et al. [224] synthesized the cubic and star-shaped Cu_2O as anode material for lithium ion batteries. Results show that the cubic Cu_2O delivers a higher discharge capacity than star-shaped Cu_2O, and has a good stability.

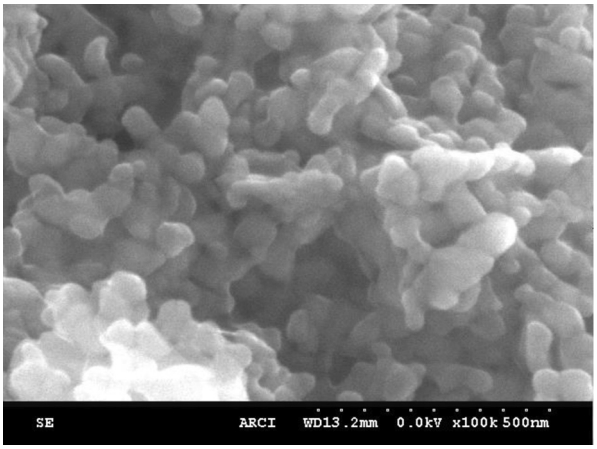

Fig. 14. SEM microstructure of nano ZnO/C composite powder [211].

CuO nanostructures were used as pseudocapacitor electrode materials and exhibited superior performance in terms of specific capacitance, cyclability, energy density, and power density [225,226].

Qiu et al. [227] synthesized copper oxide nanostructures by facile microwave-assisted hydrothermal reactions using $Cu(CH_3COO)_2$/urea and $Cu(NO_3)_2$/urea aqueous solutions, respectively. The synthesized copper oxide nanomaterials exhibited excellent pseudocapacitance behaviour in potassium hydroxide solution.

4.10. Vanadium oxide

Vanadium oxides in various forms (e.g., $H_2V_3O_8$, V_2O_5) are widely studied as electrode material for Li-ion batteries (LIBs) [228,229] and electrochemical capacitors (ECs) in organic electrolytes [230]. Since several vanadium oxides with layered structures show the redox intercalation ability for various cations, these materials are considered as an important electrode in developing high energy density LIBs [231] and high power ECs [232]. Many chemical routes, such as hydrothermal synthesis [228,233], sol–gel method [234], and electrochemical deposition [232] have been developed to prepare vanadium oxides.

Hydrous vanadium oxides deposited at potentials equal to/more positive than 0.4 V showed promising capacitive performance in aqueous media containing concentrated Li ions. Such vanadium oxides have been found to possess highly reversible Li-ion intercalation/de-intercalation behaviour in 12 M LiCl between −0.2 and 0.8 V [232]. Since the tunnels of Li-ion diffusion should be affected by the crystallinity of vanadium oxides [235], Li et al. [50] used the microwave-assisted hydrothermal synthesis (MAHS) method to synthesize vanadium oxide nanocrystals in order to shorten the Li-ion diffusion length. Moreover, this work demonstrated the idea that doping of Li ions could tune the Li-ion diffusion tunnels within vanadium oxide nanocrystals in order to enhance Li-ion intercalation/deintercalation rate for the application of ECs.

Vanadium oxides ($VO_x \cdot nH_2O$) with long cycle-life for Li-ion supercapacitors have been successfully synthesized by means of microwave-assisted hydrothermal synthesis (MAHS) method, a faster and more energy-saving method than the conventional hydrothermal synthesis. Such oxides show capacitor like, lithium-ion intercalation/de-intercalation responses in aqueous media. Although electrochemical activation is required to reveal the capacitor-like behaviour of $VO_x \cdot nH_2O$, doping Li ions by adding LiCl

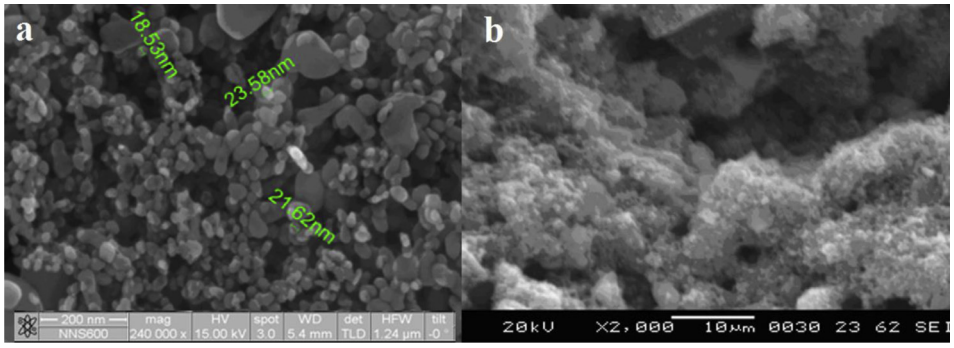

Fig. 15. (a) FESEM image of ZnO, (b) SEM image of ZnO-activated carbon composite [215].

into the precursor solution not only effectively shortens the activation time, but also enhances the specific capacitance of $VO_x \cdot nH_2O$.

4.11. Titanium oxide

Titanium oxide (TiO_2) has been found to be an alternative for other metal oxides. Titania nanotubes have been obtained by alkaline hydrothermal treatment [236]. The TiO_2 particles so formed were subjected to microwave heating in different microwave power as well as different time [69]. TiO_2 is a good dielectric material and exhibits faradaic capacitance. Therefore, the combination of high surface area activated carbon with large specific capacity of TiO_2 is expected to form a composite with both the faradaic capacitance of the metal oxide and the double layer capacitance of the activated carbon. TiO_2 nanoparticles have been prepared by a microwave assisted synthesis method and TiO_2/AC nanocomposite used as electrodes with specific capacitance of 122 F g^{-1}. The power and energy density of TiO_2/AC supercapacitor show 2.574 W g^{-1} and 92.74 Wh g^{-1}, respectively [237].

4.12. Mixed metal oxides/hydroxides

To increase the power delivery, at least by one order of magnitude higher than existing capacitors, metal oxides and mixed metal oxides have been introduced as electrodes which also deliver pseudo-capacitance. For an ideal double layer capacitor, the charge is transferred into the double layer and there are no faradaic reactions between the solid material and the electrolyte. In this case, the capacitance is constant and independent of voltage. On the other hand, for capacitors that use metal oxides, pseudo-capacitance, due to faradaic reactions between the solid material and the electrolyte, it is voltage dependent. Lead Pb/Ru pyrochlore ($Pb_2Ru_2O_{6.5}$) has been synthesized as a new electrode material for aqueous electrolyte capacitors and the performance is similar to ruthenium oxide electrodes [238]. The $MnFe_2O_4$/graphene nanocomposite supercapacitor shows an energy density of 25.9 Wh kg^{-1} at a power density of 225 W kg^{-1} and an energy density of 18.1 Wh kg^{-1} at a power density of 14.4 kW kg^{-1}, indicating an excellent power capability [239]. A novel $MnSn(OH)_6$/graphene nanocomposite was produced by a co-precipitation method, with the potential application for electrochemical energy storage with maximum capacitance of 31.2 F g^{-1} [240].

Jayalakshmi et al. [241] synthesized nano-SnO_2–Al_2O_3 and SnO_2–Al_2O_3–carbon composites via a simple single step hydrothermal route. In 0.1 M NaCl solutions, the electrochemical double layer capacitance of SnO_2–Al_2O_3 is much greater than of the pure SnO_2 and the electrode is electrochemically and chemically stable even after cycling 1000 times. The performance of the carbon added composites is better than SnO_2 but lower than SnO_2–Al_2O_3. Veerasubramani et al. [242] reported a facile sonochemical approach to the synthesis of cobalt molybdate ($CoMoO_4$) nanostructures and their application as electrodes for supercapacitors. A thin film binder-free Co–Mn composite oxide ($MnCo_2O_4$) electrode is fabricated by using electroless electrolytic (EE) techniques that used for supercapacitor. The EE electrode yields a specific capacitance of 240 F g^{-1} at 74 A g^{-1} with an energy density of 21 Wh kg^{-1} and 51.6 kW kg^{-1} of power density [57]. As a potential functional material, zinc cobaltite ($ZnCo_2O_4$) has been investigated for applications as Li-ion batteries anode materials [243–245].

Nickel cobaltite ($NiCo_2O_4$), a type of spinel oxide, has attracted considerable interest due to its low cost. It seems to be the most promising material in the alkaline solution and negative electrode of lithium ion batteries [246]. Several methods have been used to prepare $NiCo_2O_4$, such as hydroxide decomposition, electrospinning technique, and sol–gel [247]. Microwave-assisted hydrothermal process is a recent technique to prepare nanocrystalline oxides in very shorter durations. Only few papers deal with $NiCo_2O_4$ nanoparticles used in supercapacitors by microwave-assisted hydrothermal method. Tseng et al. [248] have extended this microwave assisted hydrothermal synthesis to prepare $NiCo_2O_4$ nanoparticles for its application for supercapacitors. $NiCo_2O_4$ nanoparticles show a high-specific capacitance of 332.8 F g^{-1} under a mass loading of 2 mg cm^{-1} within −0.5 and 0.5 V at a scan rate of 100 mV s^{-1} in a 0.5 M H_2SO_4 solution.

Among these composite materials, Co–Ni hydroxides have drawn increasing attention because the introduction of cobalt can not only reduce the resistance of the electrode and raise the oxygen over potential, but also participate in the electrochemical redox reaction [249,250]. Particularly, layered transition-metal hydroxides with large interlayer spacing display desirable electrochemical activity derived from their redox nature and better accessibility for the reaction species [251]. The similarities between Ni and Co offer opportunities to yield hybrid materials by the widely applied technological doping strategy. If Ni and Co are co-incorporated in the host layer, an improved capacity and cycling stability may be expected in comparison with monometallic hydroxides, which therefore offers an effective way to achieve high electrochemical performance [248,252–254]. Various synthetic approaches have been adopted or improved for preparing $Co(OH)_2$ and $Ni(OH)_2$ nanomaterials, such as: sonochemical [21], solvothermal [22,23], and hydrothermal process [24,25]. A network of $Co_xNi_yAl_z$ layered triple hydroxides (LTHs) nanosheets has been prepared by the potentiostatic deposition process. The maximum specific capacitance of 1263 F g^{-1} is obtained for $Co_{0.59}Ni_{0.21}Al_{0.20}$LTH [255]. Ternary Ni–Co–Cu oxy-hydroxide nanosheets with excellent pseudocapacitive characteristics have been prepared by cathodic deposition [256]. Among these strategies, the microwave-assisted

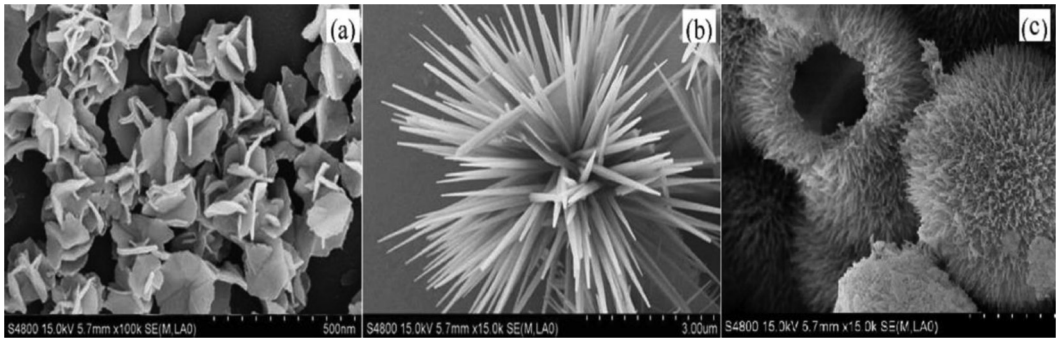

Fig. 16. FESEM images of single $Ni(OH)_2$ (a), $Co(OH)_2$ (b), and $Ni(OH)_2$–$Co(OH)_2$ composites [253].

route is a fast, simple, and effective method synthesize transition metal hydroxides due to its clean, cheap, and efficient heating [248,252,253,257,258].

A microwave-assisted reflux method has been used to rapidly synthesize CoAl-layered double hydroxide (CoAl-LDH)/graphene oxide composite. A maximum specific capacitance of 772 F g^{-1} is obtained at 1 A g^{-1} in 6 M KOH solution for the composite containing 12.9% GO. Moreover, the composite exhibits excellent long cycle life with about 73% specific capacitance retained at 6 A g^{-1} after 10,000 cycles [64].

Urchin-like $Ni(OH)_2$–$Co(OH)_2$ hollow microspheres have been successfully synthesized by a microwave-incorporated hydrothermal method. The $Ni(OH)_2$–$Co(OH)_2$ hollow microspheres achieve a high specific capacitance of 2164 F g^{-1} at 1 A g^{-1} and long-term cycle life. Electrochemical data reveals that the $Ni(OH)_2$–$Co(OH)_2$ hollow microspheres exhibit much better electrochemical reversibility and specific capacitance retention than that of the single $Ni(OH)_2$ or $Co(OH)_2$, based on peak potential difference, symmetry of charge–discharge curves, and specific capacitances at high charge–discharge rates. For comparison, FESEM images of single $Ni(OH)_2$ and $Co(OH)_2$ are shown in Fig. 16 [253]. By using the microwave-incorporated hydrothermal method, uniform flower-like $Ni(OH)_2$ nanosheets with a size of 150–250 nm are presented (Fig. 16(a)), while the $Co(OH)_2$ sample shows needle-like ordered nanowires (Fig. 16(b)). Thus, it can be concluded that the urchin-like hollow microspheres architecture of the $Ni(OH)_2$–$Co(OH)_2$ composite may come from the synthetic multi-component effect of $Ni(OH)_2$ and $Co(OH)_2$ (Fig. 16(c)). This sort of controllable hollow-structured nanomaterials may have high electrochemical properties because of their well-defined interior voids, high specific surface area, good electronic conductivity, and structural stability [253]. The hybrid $Co_{0.2}Ni_{0.8}(OH)_2$ hexagonal nanosheets are synthesized via a facile microwave-assisted and delivered a high capacity of above 1170 F g^{-1} at a current density of 4 A g^{-1} [258].

5. Conclusions

Supercapacitors or Double-layer Capacitors (DLC) are considered as power sources, with a power density between 5 and 15 kW kg^{-1}. In fact, supercapacitors are direct electrical storage components. As a matter of fact, the electrical power is directly stored as electrostatic power, without any energy conversion. Therefore, the stored electrical power can be quickly supplied by supercapacitors. Although their capacity of specific energy is rather low (about 5–10 Wh kg^{-1}), supercapacitors are able to provide high levels of current and power for about one million of charge/discharge cycles. In this way, supercapacitors are complementary to other electrical sources, whose dynamic behaviour and stored energy capability are different.

Now, a variety of carbonaceous materials with high surface area, suitable surface chemistry, and suitable pore structure are expected to be applied as excellent electrode materials to enhance EDLC with high performance. Although this capacitance per unit area is low ~10–30 mF cm^{-2}, it can be appreciably improved by the use of materials with high specific surface areas. In order to improve the wettability and capacitive performance of carbonaceous materials, some chemical surface modifications have been conducted. Metal oxide/hydroxide particles such as ruthenium oxide, manganese oxide, cobalt oxide, nickel oxide and mixed metal oxides/hydroxide have been deposited on carbon to improve the specific capacitance of electrodes. The metal oxides/hydroxides play a crucial role in enhancing the capacitance of electrodes through fast faradaic pseudocapacitance effects. Moreover, the improvement in electrical conductivity of electrodes when using metal is of importance for promoting the capacitive behaviour of carbon capacitors.

As a simple, quick, inexpensive, uniform and energy-efficient heating method, microwave irradiation has been widely used in industry and academia to synthesize such porous materials. In recent years, microwave-assisted synthesis of inorganic materials has received great attention as it can shorten the reaction time from several hours to a few minutes, with enormous energy savings. The greatest advantage of microwave heating is that it can heat a substance uniformly, leading to a more homogeneous nucleation and a shorter crystallization time compared with those for conventional heating. Microwave heating has been introduced to assist in the synthesis of metal oxide/hydroxide materials recently.

This review, illustrates that microwave synthesis approach can have wide implications in fine-tuning surface properties of metal oxide/hydroxide materials for energy storage applications.

Acknowledgements

The authors are grateful to the Universiti Teknologi Malaysia (UTM), Research Management Centre (RMC) and Post-Doctoral Program for financial support given to Dr. Soheila Faraji.

References

[1] G. Wang, L. Zhang, J. Zhang, Chem. Soc. Rev. 41 (2012) 797–828.
[2] N. Devillers, S. Jemei, M.-C. Pera, D. Bienaime, F. Gustin, J. Power Sources 246 (2014) 596–608.
[3] Y. Zhang, H. Feng, X. Wu, L. Wang, A. Zhang, T. Xia, H. Dong, X. Li, L. Zhang, Int. J. Hydrogen Energy 34 (2009) 4889–4899.
[4] A. Burke, J. Power Sources 91 (2000) 37–50.
[5] M. Nakamura, M. Nakanishi, K. Yamamoto, J. Power Sources 60 (1996) 225–231.
[6] C.D. Lokhande, D.P. Dubal, O.-S. Joo, Curr. Appl. Phys. 11 (2011) 255–270.
[7] M. Inagaki, H. Konno, O. Tanaike, J. Power Sources 195 (2010) 7880–7903.
[8] P. Simon, Y. Gogotsi, Nat. Mater. 7 (2008) 845–855.
[9] A. Davies, A. Yu, Can. J. Chem. Eng. 89 (2011) 1342–1357.
[10] M. Armand, J.M. Tarascon, Nature 451 (2008) 652–657.

[11] K. Rand, Mater. Res. Soc. Bull. 32 (2007), 464.
[12] R. Kotz, M. Carlen, Electrochim. Acta 45 (2000) 2483–2498.
[13] A. Burke, M. Miller, J. Power Sources 196 (2011) 514–522.
[14] S. Chandrasekaran, S. Ramanathan, T. Basak, Food Res. Int. 52 (2013) 243–261.
[15] Z. Abubakar, A.A. Salema, F.N. Ani, Bioresour. Technol. 128 (2013) 578–585.
[16] F. Motasemi, F.N. Ani, Renewable Sustainable Energy Rev. 16 (2012) 4719–4733.
[17] F. Motasemi, M.T. Afzal, Renewable Sustainable Energy Rev. 28 (2013) 317–330.
[18] S. Mutyala, C. Fairbridge, J.R.J. Pare, J.M.R. Belanger, S. Ng, R. Hawkins, Fuel Process. Technol. 91 (2010) 127–135.
[19] H. Shang, W. Du, Z. Liu, H. Zhang, J. Ind. Eng. Chem. 19 (2013) 1061–1068.
[20] S.-E. Park, J.-S. Chang, Y. Hwang, D. Kim, S. Jhung, J. Hwang, Catal. Surv. Asia 8 (2004) 91–110.
[21] J. Wang, B. Niu, G. Du, R. Zeng, Z. Chen, Z. Guo, S. Dou, Mater. Chem. Phys. 126 (2011) 747–754.
[22] S. Vijayakumar, A.K. Ponnalagi, S. Nagamuthu, G. Muralidharan, Electrochim. Acta 106 (2013) 500–505.
[23] S. Nagamuthu, S. Vijayakumar, G. Muralidharan, Energy Fuels 27 (2013) 3508–3515.
[24] B. Ming, J. Li, F. Kang, G. Pang, Y. Zhang, L. Chen, J. Xu, X. Wang, J. Power Sources 198 (2012) 428–431.
[25] Y. Yao, Z. Yang, H. Sun, S. Wang, Ind. Eng. Chem. Res. 51 (2012) 14958–14965.
[26] H. Wang, L. Zhang, X. Tan, C.M.B. Holt, B. Zahiri, B.C. Olsen, D. Mitlin, J. Phys. Chem. C 115 (2011) 17599–17605.
[27] C.-C. Hu, Y.-H. Huang, K.-H. Chang, J. Power Sources 108 (2002) 117–127.
[28] J. Hendrikse, W. Olthuis, P. Bergveld, Sens. Actuators B 53 (1998) 97–103.
[29] M. Ramani, B.S. Haran, R.E. White, B.N. Popov, J. Electrochem. Soc. 148 (2001) A374–A380.
[30] D. Choi, in: Synthesis, Structure and Electrochemical Characterization of Transition Metal Nitride Supercapacitors Derived by a Two-step Transition Metal Halide Approach, Carnegie Mellon University, Pittsburgh, 2005.
[31] B.E. Conway, W.G. Pell, J. Solid State Electrochem. 7 (2003) 637–644.
[32] D.A. Scherson, A. Palencsar, ECS Interface (Spring 2006) 17–23.
[33] W. Sun, R. Zheng, X. Chen, J. Power Sources 195 (2010) 7120–7125.
[34] H. Liu, P. He, Z. Li, Y. Liu, J. Li, Electrochim. Acta 51 (2006) 1925–1931.
[35] S. Zhao, F. Wu, L. Yang, L. Gao, A. Burke, Electrochem. Commun. 12 (2010) 242–245.
[36] M.D. Stoller, S.R. Rodney, Energy Environ. Sci. 3 (2010) 1294–1301.
[37] V. Khomenko, E. Raymundo-Pinero, F. Baguin, J. Power Sources 153 (2006) 183–190.
[38] M. Vangari, T. Pryor, L. Jiang, J. Energy Eng. 139 (2013) 72–79.
[39] J.R. Miller, P. Simon, Science 321 (2008) 651–652.
[40] Cap-XX, http://www.cap-xx.com/, (En ligne), 2013.
[41] EPCOS, http://www.epcos.com/, (En ligne), 2013.
[42] Maxwell, http://www.maxwell.com, (En ligne), 2013.
[43] Panasonic, http://www.panasonic.com/, (En ligne), 2013.
[44] S. Das, A.K. Mukhopadhyay, S. Datta, D. Basu, Bull. Mater. Sci. 31 (2008) 943–956.
[45] H.I. Lee, J.H. Kim, S.H. Joo, H. Chang, D. Seung, O.-S. Joo, D.J. Suh, W.-S. Ahn, C. Pak, J.M. Kim, Carbon 45 (2007) 2851–2854.
[46] J.-F. Zhu, Y.-J. Zhu, J. Phys. Chem. B 110 (2006) 8593–8597.
[47] Y. Wang, Z. Iqbal, S. Mitra, Carbon 44 (2006) 2804–2808.
[48] Z. An, W. Tang, C.J. Hawker, G.D. Stucky, J. Am. Chem. Soc. 128 (2006) 15054–15055.
[49] K.-H. Chang, C.-C. Hu, C.-M. Huang, Y.-L. Liu, C.-I. Chang, J. Power Sources 196 (2011) 2387–2392.
[50] J.-M. Li, K.-H. Chang, T.-H. Wu, C.-C. Hu, J. Power Sources 224 (2013) 59–65.
[51] C. Gabriel, S. Gabriel, E.H. Grant, B.S.J. Halsteed, D.P. Mingos, Chem. Soc. Rev. 27 (1998) 213–224.
[52] D.M.P. Mingos, D.R. Baghurst, Chem. Soc. Rev. 20 (1991) 1–47.
[53] K.J. Rao, B. Vaidhyanathan, M. Ganguli, P.A. Ramakrishnan, Chem. Mater. 11 (1999) 882–895.
[54] H. Xia, M.O. Lai, L. Lu, JOM 63 (2011) 54–59.
[55] J.N. Broughton, M.J. Brett, Electrochim. Acta 50 (2005) 4814–4819.
[56] R.N. Reddy, R.G. Reddy, J. Power Sources 132 (2004) 315–320.
[57] J. Gomez, E.E. Kalu, J. Power Sources 230 (2013) 218–224.
[58] A.L.M. Reddy, F.E. Amitha, I. Jafri, S. Ramaprabhu, Nanoscale Res. Lett. 3 (2008) 145–151.
[59] W.-J. Liu, Y.-M. Dai, J.-M. Jehng, J. Taiwan Inst. Chem. Eng. 49 (2014) 475–480.
[60] K. Lota, A. Sierczynska, G. Lota, Int. J. Electrochem. (2011) 1–6.
[61] J. Jiang, J. Liu, R. Ding, J. Zhu, Y. Li, A. Hu, X. Li, X. Huang, ACS Appl. Mater. Interfaces 3 (2011) 99–103.
[62] N. Behm, D. Brokaw, C. Overson, D. Peloquin, J. Poler, J. Mater. Sci. 48 (2013) 1711–1716.
[63] D. Antiohos, K. Pingmuang, M.S. Romano, S. Beirne, T. Romeo, P. Aitchison, A. Minett, G. Wallace, S. Phanichphant, J. Chen, Electrochim. Acta 101 (2013) 99–108.
[64] J. Fang, M. Li, Q. Li, W. Zhang, Q. Shou, F. Liu, X. Zhang, J. Cheng, Electrochim. Acta 85 (2012) 248–255.
[65] C.-L. Liu, K.-H. Chang, C.-C. Hu, W.-C. Wen, J. Power Sources 217 (2012) 184–192.
[66] S.H. Jhung, T. Jin, Y.K. Hwang, J.S. Chang, Chem. Eur. J. 16 (2007) 4410–4417.
[67] Y. Hu, C. Liu, Y. Zhang, N. Ren, Y. Tang, Microporous Mesoporous Mater. 119 (2009) 306–314.
[68] I. Bilecka, M. Niederberger, Nanoscale Res. Lett. 2 (2010) 1358–1374.
[69] J.-K. Lee, H.M. Pathan, K.-D. Jung, O.-S. Joo, J. Power Sources 159 (2006) 1527–1531.
[70] C. Niu, E.K. Sichel, R.R. Hoch, D.D. Moy, H. Tennent, Appl. Phys. Lett. 70 (1997) 1480–1482.
[71] W.-C. Fang, O. Chyan, C.-L. Sun, C.-T. Wu, C.-P. Chen, K.-H. Chen, L.-C. Chen, J.-H. Huang, Electrochem. Commun. 9 (2007) 239–244.
[72] C.-C. Hu, K.-H. Chang, C.-C. Wang, Electrochim. Acta 52 (2007) 4411–4418.
[73] C.-C. Hu, W.-C. Chen, Electrochim. Acta 49 (2004) 3469–3477.
[74] S. Yan, H. Wang, P. Qu, Y. Zhang, Z. Xiao, Synth. Met. 159 (2009) 158–161.
[75] X. Wang, W.B. Yue, M.S. He, M.H. Liu, J. Zhang, Z.F. Liu, Chem. Mater. 16 (2004) 799–805.
[76] L. Li, K.H. Seng, H. Liu, I.P. Nevirkovets, Z. Guo, Electrochim. Acta 87 (2013) 801–808.
[77] J. Gao, M.A. Lowe, H.D. Abruna, Chem. Mater. 23 (2011) 3223–3227.
[78] F. Naamoune, B. Messaoudi, A. Kahoul, N. Cherchour, A. Pailleret, H. Takenouti, Ionics 18 (2012) 365–370.
[79] G. Laugel, J. Arichi, H. Guerba, M. Molire, A. Kiennemann, F. Garin, B. Louis, Catal. Lett. 125 (2008) 14–21.
[80] S.W. Donne, A.F. Hollenkamp, B.C. Jones, J. Power Sources 195 (2010) 367–373.
[81] E.C. Rios, A.V. Rosario, R.M.Q. Mello, L. Micaroni, J. Power Sources 163 (2007) 1137–1142.
[82] G.A. Kriegsmann, J. Appl. Phys. 71 (1992) 1960–1966.
[83] M. Ghaemi, F. Ataherian, A. Zolfaghari, S.M. Jafari, Electrochim. Acta 53 (2008) 4607–4614.
[84] Z. Fan, J. Chen, B. Zhang, B. Liu, X. Zhong, Y. Kuang, Diamond Relat. Mater. 17 (2008) 1943–1948.
[85] G.A. Tompsett, W.C. Conner, K.S. Yngvesson, ChemPhysChem 7 (2006) 296–319.
[86] L. Chen, D. Zhu, Solid State Sci. 27 (2014) 69–72.
[87] N. Chen, K. Wang, X. Zhang, X. Chang, L. Kang, Z.-H. Liu, Colloids Surf. A 387 (2011) 10–16.
[88] S. Chou, F. Cheng, J. Chen, J. Power Sources 162 (2006) 727–734.
[89] D.P. Dubal, D.S. Dhawale, T.P. Gujar, C.D. Lokhande, Appl. Surf. Sci. 257 (2011) 3378–3382.
[90] X. Wang, X. Wang, W. Huang, P.J. Sebastian, S. Gamboa, J. Power Sources 140 (2005) 211–215.
[91] S.K. Meher, G.R. Rao, J. Power Sources 215 (2012) 317–328.
[92] S.W. Lee, J. Kim, S. Chen, P.T. Hammond, Y. Shao-Horn, ACS Nano 4 (2010) 3889–3896.
[93] J. Yan, Z. Fan, T. Wei, J. Cheng, B. Shao, K. Wang, L. Song, M. Zhang, J. Power Sources 194 (2009) 1202–1207.
[94] P. Yu, X. Zhang, Y. Chen, Y. Ma, Z. Qi, Mater. Chem. Phys. 118 (2009) 303–307.
[95] A. Bello, O.O. Fashedemi, M. Fabiane, J.N. Lekitima, K.I. Ozoemena, N. Manyala, Electrochim. Acta 114 (2013) 48–53.
[96] Y. Li, J. Wang, Y. Zhang, M.N. Banis, J. Liu, D. Geng, R. Li, X. Sun, J. Colloid Interface Sci. 369 (2012) 123–128.
[97] E.K. Nyutu, C.-H. Chen, S. Sithambaram, V.M.B. Crisostomo, S.L. Suib, J. Phys. Chem. C 112 (2008) 6786–6793.
[98] H. Huang, S. Sithambaram, C.-H. Chen, C. Kingondu Kithongo, L. Xu, A. Iyer, H.F. Garces, S.L. Suib, Chem. Mater. 22 (2010) 3664–3669.
[99] X. Zhang, X. Sun, H. Zhang, D. Zhang, Y. Ma, Electrochim. Acta 87 (2013) 637–644.
[100] Z. Chen, J. Li, Y. Chen, Y. Zhang, G. Xu, J. Yang, Y. Feng, Particuology (2013) http://dx.doi.org/10.1016/j.partic.2012.12.008.
[101] P. Ragupathy, H.N. Vasan, N. Munichandraiah, Mater. Chem. Phys. 124 (2010) 870–875.
[102] Y. Xiao, Q. Zhang, J. Yan, T. Wei, Z. Fan, F. Wei, J. Electroanal. Chem. 684 (2012) 32–37.
[103] Z. Fan, Z. Qie, T. Wei, J. Yan, S. Wang, Mater. Lett. 62 (2008) 3345–3348.
[104] P.C. Chen, G.Z. Shen, Y. Shi, H.T. Chen, C.W. Zhou, ACS Nano 4 (2010) 4403–4411.
[105] Z. Fan, M. Xie, X. Jin, J. Yan, T. Wei, J. Electroanal. Chem. 659 (2011) 191–195.
[106] W. Yang, Z. Gao, J. Wang, B. Wang, Q. Liu, Z. Li, T. Mann, P. Yang, M. Zhang, L. Liu, Electrochim. Acta 69 (2012) 112–119.
[107] J. Yan, Z. Fan, T. Wei, W. Qian, M. Zhang, F. Wei, Carbon 48 (2010) 3825–3833.
[108] K.V. Sankar, S.T. Senthilkumar, L.J. Berchmans, C. Sanjeeviraja, R.K. Selvan, Appl. Surf. Sci. 259 (2012) 624–630.
[109] K. Chen, Y.D. Noh, S. Lin, S. Komarneni, D. Xue, Mater. Focus 2 (2013) 86–91.
[110] K. Chen, D. Xue, CrystEngComm 15 (2013) 1739–1746.
[111] K. Chen, D. Xue, CrystEngComm 14 (2012) 8068–8075.
[112] B. Dunn, H. Kamath, J.M. Tarascon, Science 334 (2011) 928–935.
[113] K. Chen, Y. Dong Noh, W. Huang, J. Ma, S. Komarneni, D. Xue, Ceram. Int. 2 (2014) 2877–2884.
[114] P. Justin, S.K. Meher, G.R. Rao, J. Phys. Chem. C 114 (2010) 5203–5210.
[115] S.K. Meher, P. Justin, G.R. Rao, Electrochim. Acta 55 (2010) 8388–8396.
[116] K.W. Nam, K.B. Kim, J. Electrochem. Soc. 149 (2002) A346–A354.
[117] J.W. Lang, L.B. Kong, W.J. Wu, Y.C. Luo, L. Kang, Chem. Commun. 35 (2008) 4213–4215.
[118] S. Xiong, C. Yuan, X. Zhang, Y. Qian, CrystEngComm 13 (2011) 626–632.

[119] C. Yuan, X. Zhang, L. Su, B. Gao, L. Shen, J. Mater. Chem. 19 (2009) 5772–5777.
[120] S. Ding, T. Zhu, J.S. Chen, Z. Wang, C. Yuan, X.W. (David) Lou, J. Mater. Chem. 21 (2011) 6602–6606.
[121] M.S. Wu, M. Wang, Chem. Commun. 46 (2010) 6968–6970.
[122] Y.Z. Zheng, H.Y. Ding, M.L. Zhang, Mater. Res. Bull. 44 (2009) 403–407.
[123] L. Xu, Y.-S. Ding, C.-H. Chen, L. Zhao, C. Rimkus, R. Joesten, S.L. Suib, Chem. Mater. 20 (2007) 308–316.
[124] D. Obermayer, B. Gutmann, C.O. Kappe, Angew. Chem. Int. Ed. 48 (2009) 8321–8324.
[125] Y. Ren, L.J. Gao, J. Am. Ceram. Soc. 93 (2010) 3560–3564.
[126] C.Y. Cao, W. Guo, Z.M. Cui, W.G. Song, W. Cai, J. Mater. Chem. 21 (2011) 3204–3209.
[127] S.K. Meher, P. Justin, G.R. Rao, ACS Appl. Mater. Interfaces 3 (2011) 2063–2073.
[128] S. Vijayakumar, S. Nagamuthu, G. Muralidharan, ACS Sustainable Chem. Eng. 1 (2013) 1110–1118.
[129] S.R. Ovshinsky, M.A. Fetcenko, J. Ross, Science 260 (1993) 176–181.
[130] J.-W. Lang, L.-B. Kong, W.-J. Wu, M. Liu, Y.-C. Luo, L. Kang, J. Solid State Electrochem. 13 (2008) 333–340.
[131] C. Coudun, J.F. Hochepied, J. Phys. Chem. 109 (2005) 6069–6074.
[132] X.Y. Wang, H. Luo, P.V. Parkhutik, A.C. Millan, E. Matveeva, J. Power Sources 115 (2003) 153–160.
[133] L.X. Yang, Y.J. Zhu, H. Tong, Z.H. Liang, L. Li, L. Zhang, J. Solid State Chem. 180 (2007) 2095–2101.
[134] T.N. Ramesh, P.V. Kamath, J. Power Sources 156 (2006) 655–661.
[135] R. Yang, L. Gao, J. Colloid Interface Sci. 297 (2006) 134–137.
[136] F.Y.C.S.L. Chou, J. Chen, Eur. J. Inorg. Chem. 22 (2005) 4035–4039.
[137] W.Y. Li, S.Y. Zhang, J. Phys. Chem. B 109 (2005) 19094–19098.
[138] K. Matsui, T. Kyotani, A. Tomita, Adv. Mater. 14 (2002) 1216–1219.
[139] Z.H. Liang, Y.J. Zhu, X.L. Hu, Phys. Chem. B 108 (2004) 3488–3491.
[140] D.L. Chen, L. Gao, Chem. Phys. Lett. 405 (2005) 159–164.
[141] M. Meyer, A. Bée, D. Talbot, V. Cabuil, J.M. Boyer, B. Répetti, R. Garrigos, J. Colloid Interface Sci. 277 (2004) 309–315.
[142] Y. Wang, Q.S. Zhu, H.G. Zhang, Chem. Commun. 41 (2005) 5231–5233.
[143] D.B. Wang, C.X. Song, Z.X. Hu, X. Fu, J. Phys. Chem. B 109 (2005) 1125–1129.
[144] L.X. Yang, Y.J. Zhu, H. Tong, Z.H. Liang, W.W. Wang, Cryst. Growth Des. 7 (2007) 2716–2719.
[145] P. Oliva, J. Leonardi, J.F. Laurent, C. Delmas, J.J. Braconnier, M. Figlarz, F. Fievet, A. de Guibert, J. Power Sources 8 (1982) 229–255.
[146] R.A. Huggins, H. Prinz, M. Wohlfahrt-Mehrens, L. Jorissen, W. Witschel, Solid State Ionics 70–71 (1994) 417–424.
[147] X.-Z. Fu, Q.-C. Xu, R.-Z. Hu, B.-X. Pan, J.-D. Lin, D.-W. Liao, J. Power Sources 164 (2007) 916–920.
[148] H. Chen, J.M. Wang, T. Pan, Y.L. Zhao, J.Q. Zhang, C.N. Cao, J. Power Sources 143 (2005) 243–255.
[149] Y. Tang, Y. Liu, S. Yu, Y. Zhao, S. Mu, F. Gao, Electrochim. Acta 123 (2013) 158–166.
[150] J. Ji, L.L. Zhang, H. Ji, Y. Li, X. Zhao, X. Bai, F. Xiaobin Fan, F. Zhang, R.S. Ruoff, ACS Nano 7 (2013) 6237–6243.
[151] B.P. Bastakoti, H.-S. Huang, L.-C. Chen, K.C.W. Wu, Y. Yamauchi, Chem. Commun. 48 (2012) 9150–9152.
[152] J.H. Park, O.O. Park, K.H. Shin, C.S. Jin, J.H. Kim, Electrochem Solid State Lett. 5 (2002) H7–H10.
[153] Q. Huang, X. Wang, J. Li, C. Dai, S. Gamboa, P.J. Sebastian, J. Power Sources 164 (2007) 425–429.
[154] Z. Tang, C.-h. Tang, H.A. Gong, Adv. Funct. Mater. 22 (2012) 1272–1278.
[155] L.L. Zhang, Z. Xiong, X.S.A. Zhao, J. Power Sources 222 (2013) 326–332.
[156] S. Yang, X. Wu, C. Chen, H. Dong, W. Hu, X. Wang, Chem. Commun. 48 (2012) 2773–2775.
[157] H. Wang, Y. Liang, T. Mirfakhrai, Z. Chen, H.S. Casalongue, H. Dai, Nano Res. 4 (2011) 729–736.
[158] H.L. Wang, H.S. Casalongue, Y.Y. Liang, H.J. Dai, J. Am. Chem. Soc. 132 (2010) 7472–7477.
[159] S. Min, C. Zhao, G. Chen, X. Qian, Electrochim. Acta 115 (2014) 155–164.
[160] J. Yan, Z. Fan, W. Sun, G. Ning, T. Wei, Q. Zhang, R. Zhang, L. Zhi, F. Wei, Adv. Funct. Mater. 22 (2012) 2632–2641.
[161] X. Tian, C. Cheng, L. Qian, B. Zheng, H. Yuan, S. Xie, D. Xiao, M.M.F. Choi, J. Mater. Chem. 22 (2012) 8029–8036.
[162] P.S. Patil, L.D. Kadam, C.D. Lokhande, Thin Solid Films 272 (1996) 29–32.
[163] R. Xu, J. Wang, Q. Li, G. Sun, E. Wang, S. Li, J. Gu, M. Ju, J. Solid State Chem. 182 (2009) 3177–3182.
[164] Z. Gui, J. Zhu, Y. Hu, Mater. Chem. Phys. 124 (2010) 243–247.
[165] S. Thota, A. Kumar, J. Kumar, Mater. Sci. Eng. B 164 (2009) 30–37.
[166] G.-L. Xu, J.-T. Li, L. Huang, W. Lin, S.-G. Sun, Nano Energy 2 (2013) 394–402.
[167] J. Pal, P. Chauhan, Mater. Charact. 61 (2010) 575–579.
[168] S.M. Islam, A.S. Roy, S. Dalapati, R. Saha, P. Mondal, K. Ghosh, S. Chatterjee, K. Sarkar, N. Guchhait, P. Mitra, J. Mol. Catal. A Chem. 380 (2013) 94–103.
[169] S. Iyer, V.V. Thakur, J. Mol. Catal. A Chem. 157 (2000) 275–278.
[170] L.M. Apatiga, V.M. Castano, Thin Solid Films 496 (2006) 576–579.
[171] R.M. Al-Tuwirqi, A.A. Al-Ghamdi, F. Al-Hazmi, F. Alnowaiser, A.A. Al-Ghamdi, N.A. Aal, F. El-Tantawy, Superlattices Microstruct. 50 (2011) 437–448.
[172] M.J. Deng, F.L. Huang, I.W. Sun, W.T. Tsai, J.K. Chang, Nanotechnology 20 (2009) 175602–175612.
[173] J. Yan, T. Wei, W. Qiao, B. Shao, Q. Zhao, L. Zhang, Z. Fan, Electrochim. Acta 55 (2010) 6973–6978.
[174] P. Shi, X. Dai, H. Zheng, D. Li, W. Yao, C. Hu, Chem. Eng. J. 240 (2014) 264–270.
[175] V.R. Mate, M. Shirai, C.V. Rode, Catal. Commun. 33 (2013) 66–69.
[176] D. Patil, P. Patil, V. Subramanian, P.A. Joy, H.S. Potdar, Talanta 81 (2010) 37–43.
[177] A.A. Ensafi, M. Jafari-Asl, B. Rezaei, Talanta 103 (2013) 322–329.
[178] A.H. Hill, A. Harrison, C. Ritter, W. Yue, W. Zhou, J. Magn. Magn. Mater. 323 (2011) 226–231.
[179] G. Ji, Z. Gong, W. Zhu, M. Zheng, S. Liao, K. Shen, J. Liu, J. Cao, J. Alloys Compd. 476 (2009) 579–583.
[180] K.T. Nam, D.W. Kim, P.J. Yoo, C.Y. Chiang, N. Meethong, P.T. Hammond, Y.M. Chiang, A.M. Belcher, Science 312 (2006) 885–888.
[181] L. Hu, Q. Peng, Y. Li, J. Am. Chem. Soc. 130 (2008) 16136–16137.
[182] S.-L. Chou, J.-Z. Wang, H.-K. Liu, S.-X. Dou, J. Power Sources 182 (2008) 359–364.
[183] Y. Gao, S. Chen, D. Cao, G. Wang, J. Yin, J. Power Sources 195 (2010) 1757–1760.
[184] N.D. Hould, R.F. Lobo, Chem. Mater. 20 (2008) 5807–5815.
[185] S.K. Meher, G.R. Rao, J. Phys. Chem. C 115 (2011) 25543–25556.
[186] L. Cao, F. Xu, Y.-Y. Liang, H.-L. Li, Adv. Mater. 16 (2004) 853–1857.
[187] C. Mondal, M. Ganguly, P.K. Manna, S.M. Yusuf, T. Pal, Langmuir 29 (2013) 9179–9187.
[188] A.D. Jagadale, V.S. Kumbhar, D.S. Dhawale, C.D. Lokhande, Electrochim. Acta 98 (2013) 32–38.
[189] L.-B. Kong, J.-W. Lang, M. Liu, Y.-C. Luo, L. Kang, J. Power Sources 194 (2009) 1194–1201.
[190] Z. Hu, L. Mo, X. Feng, J. Shi, Y. Wang, Y. Xie, Mater. Chem. Phys. 114 (2009) 53–57.
[191] V. Gupta, T. Kusahara, H. Toyama, S. Gupta, N. Miura, Electrochem. Commun. 9 (2007) 2315–2319.
[192] W.J. Zhou, J. Zhang, T. Xue, D.D. Zhao, H.L. Li, J. Mater. Chem. 18 (2008) 905–910.
[193] K. Chen, Y.D. Noh, R.R. Patel, W. Huang, J. Ma, K. Li, S. Komarneni, D. Xue, Ceram. Int. 40 (2014) 8183–8188.
[194] I. Jimenez, J. Arbiol, G. Dezanneau, A. Cornet, J.R. Morante, Sens. Actuators B 93 (2003) 475–485.
[195] C.-C. Huang, W. Xing, S.-P. Zhuo, Scr. Mater. 61 (2009) 985–987.
[196] C.G. Granqvist, Sol. Energy Mater. Sol. Cells 60 (2000) 201–262.
[197] Y.-H. Wang, C.-C. Wang, W.-Y. Cheng, S.-Y. Lu, Carbon 69 (2014) 287–293.
[198] Y. Cai, Y. Wang, S. Deng, G. Chen, Q. Li, B. Han, R. Han, Y. Wang, Ceram. Int. 40 (2014) 4109–4116.
[199] Y. Zhou, S. Ko, C.W. Lee, S.G. Pyo, S.-K. Kim, S. Yoon, J. Power Sources 244 (2013) 777–782.
[200] G.F. Cai, J.P. Tu, D. Zhou, X.L. Wang, C.D. Gu, Sol. Energy Mater. Sol. Cells 124 (2014) 103–110.
[201] D.-J. Kim, S.-I. Pyun, Electrochim. Acta 43 (1998) 2341–2347.
[202] J. Wang, E. Khoo, P.S. Lee, J. Phys. Chem. C 113 (2009) 9655–9658.
[203] O.-u. Nimittrakoolchai, S. Supothina, Mater. Chem. Phys. 112 (2008) 270–274.
[204] P.M.S. Monk, S.L. Chester, Electrochim. Acta 38 (1993) 1521–1526.
[205] D.B. Hernandez-Uresti, D. Sanchez-Martanez, A. Martanez-de la Cruz, S. Sepalveda-Guzmin, L.M. Torres-Martanez, Ceram. Int. 40 (2014) 4767–4775.
[206] X.T. Su, F. Xiao, J.L. Lin, J.K. Jian, Y.N. Li, Q.J. Sun, J.D. Wang, Mater. Charact. 61 (2010) 831–834.
[207] K.-H. Chang, C.-C. Hu, C.-M. Huang, Y.-L. Liu, C.-I. Chang, J. Power Sources 196 (2013) 2387–2392.
[208] Y.U. Jeong, A. Manthiram, J. Electrochem. Soc. 148 (2001) A189–A193.
[209] S. Wang, S.P. Jiang, X. Wang, Electrochim. Acta 56 (2011) 3338–3344.
[210] D. Kalpana, K.S. Omkumar, S.S. Kumar, N.G. Renganathan, Electrochim. Acta 52 (2006) 1309–1315.
[211] M. Jayalakshmi, M. Palaniappa, K. Balasubramanian, Int. J. Electrochem. Sci. 3 (2008) 96–103.
[212] T. Lu, Y. Zhang, H. Li, L. Pan, Y. Li, Z. Sun, Electrochim. Acta 55 (2010) 4170–4173.
[213] Y. Zhang, X. Sun, L. Pan, H. Li, Z. Sun, C. Sun, B.K. Tay, Solid State Ionics 180 (2009) 1525–1528.
[214] T. Lu, L. Pan, H. Li, G. Zhu, T. Lv, X. Liu, Z. Sun, T. Chen, D.H.C. Chua, J. Alloys Compd. 509 (2011) 5488–5492.
[215] M. Selvakumar, D. Krishna Bhat, A. Manish Aggarwal, S. Prahladh Iyer, G. Sravani, Phys. B 405 (2010) 2286–2289.
[216] J. Wang, Z. Gao, Z. Li, B. Wang, Y. Yan, Q. Liu, T. Mann, M. Zhang, Z. Jiang, J. Solid State Chem. 184 (2011) 1421–1427.
[217] N. Ouldhamadouche, A. Achour, I. Musa, K. Ait Aissa, F. Massuyeau, P.Y. Jouan, M. Kechouane, L. Le Brizoual, E. Faulques, N. Barreau, M.A. Djouadi, Thin Solid Films 520 (2012) 4816–4819.
[218] Z. Tan, D.H.C. Chua, J. Electrochem. Soc. 158 (2011) K112–K116.
[219] L.S. Aravinda, K.K. Nagaraja, H.S. Nagaraja, K.U. Bhat, B.R. Bhat, Electrochim. Acta 95 (2013) 119–124.
[220] Y. Haldorai, W. Voit, J.-J. Shim, Electrochim. Acta 120 (2014) 65–72.
[221] G. Wang, X. Tan, Q. Zhou, Y. Liu, M. Wang, L. Yang, Sens. Actuators B 190 (2014) 730–736.
[222] S. Bijani, M. Gabs, L. Marnez, J.R. Ramos-Barrado, J. Morales, L. Sánchez, Thin Solid Films 515 (2007) 5505–5511.
[223] H. Wang, Q. Pan, J. Zhao, G. Yin, P. Zuo, J. Power Sources 167 (2007) 206–211.
[224] C.Q. Zhang, J.P. Tu, X.H. Huang, Y.F. Yuan, X.T. Chen, F. Mao, J. Alloys Compd. 441 (2007) 52–56.
[225] G. Wang, J. Huang, S. Chen, Y. Gao, D. Cao, J. Power Sources 196 (2011) 5756–5760.

[226] X. Liu, Z. Li, Q. Zhang, F. Li, T. Kong, Mater. Lett. 72 (2012) 49–52.
[227] G. Qiu, S. Dharmarathna, Y. Zhang, N. Opembe, H. Huang, S.L. Suib, J. Phys. Chem. C 116 (2012) 468–477.
[228] K.-H. Chang, C.-C. Hu, Acta Mater. 55 (2007) 6192–6197.
[229] X. Zhou, C. Cui, G. Wu, H. Yang, J. Wu, J. Wang, G. Gao, J. Power Sources 238 (2013) 95–102.
[230] T. Kudo, Y. Ikeda, T. Watanabe, M. Hibino, M. Miyayama, H. Abe, K. Kajita, Solid State Ionics 152–153 (2002) 833–841.
[231] E. Shouji, D.A. Buttry, Langmuir 15 (1999) 669–673.
[232] C.-C. Hu, C.-M. Huang, K.-H. Chang, J. Power Sources 185 (2008) 1594–1597.
[233] J. Livage, Materials 3 (2010) 4175–4195.
[234] J. Livage, ACS Chem. Mater. 3 (1991) 578–593.
[235] Y. Wang, K. Takahashi, K.H. Lee, G.Z. Cao, Adv. Funct. Mater. 16 (2006) 1133–1144.
[236] D.S. Seo, J.K. Lee, J.H. Kim, J. Cryst. Growth 229 (2001) 428–432.
[237] M. Selvakumar, D.K. Bhat, Appl. Surf. Sci. 263 (2012) 236–241.
[238] F. Cao, J. Prakash, J. Power Sources 92 (2001) 40–44.
[239] B. Li, Y. Fu, H. Xia, X. Wang, Mater. Lett. 122 (2014) 193–196.
[240] G. Wang, X. Sun, F. Lu, Q. Yu, C. Liu, J. Lian, J. Solid State Chem. 185 (2012) 172–179.
[241] M. Jayalakshmi, N. Venugopal, K.P. Raja, M.M. Rao, J. Power Sources 158 (2006) 1538–1543.
[242] G.K. Veerasubramani, K. Krishnamoorthy, S. Radhakrishnan, N.-J. Kim, S.J. Kim, Int. J. Hydrogen Energy 39 (2014) 5186–5193.
[243] G. Zhou, J. Zhu, Y. Chen, L. Mei, X. Duan, G. Zhang, L. Chen, T. Wang, B. Lu, Electrochim. Acta 123 (2014) 450–455.
[244] X. Song, Q. Ru, B. Zhang, S. Hu, B. An, J. Alloys Compd. 585 (2014) 518–522.
[245] H. Liu, J. Wang, Electrochim. Acta 92 (2013) 371–375.
[246] R. Ding, L. Qi, H. Wang, Electrochim. Acta 114 (2013) 726–735.
[247] J.F. Marco, J.R. Gancedo, M. Gracia, J.L. Gautier, E. Rios, F.J. Berry, J. Solid State Chem. 153 (2000) 74–81.
[248] C.-C. Tseng, J.-L. Lee, Y.-M. Liu, M.-D. Ger, Y.-Y. Shu, J. Taiwan Inst. Chem. Eng. 44 (2013) 415–419.
[249] L. Xie, Z. Hu, C. Lv, G. Sun, J. Wang, Y. Li, H. He, J. Wang, K. Li, Electrochim. Acta 78 (2012) 205–211.
[250] V. Gupta, S. Gupta, N. Miura, J. Power Sources 175 (2008) 680–685.
[251] X. Liu, R. Ma, Y. Bando, T. Sasaki, Adv. Mater. 24 (2012) 2148–2153.
[252] Y. Tao, Z. Haiyan, L. Ruiyi, L. Zaijun, L. Junkang, W. Guangli, G. Zhiquo, Electrochim. Acta 111 (2013) 71–79.
[253] J. Xu, Y. Dong, J. Cao, B. Guo, W. Wang, Z. Chen, Electrochim. Acta 114 (2013) 76–82.
[254] Y.Y. Liang, S.J. Bao, H.L. Li, J. Solid State Electrochem. 11 (2007) 571–576.
[255] V. Gupta, S. Gupta, N. Miura, J. Power Sources 189 (2009) 1292–1295.
[256] C.-H. Lien, C.-C. Hu, C.-T. Hsu, D.S.-H. Wong, Electrochem. Commun. 34 (2013) 323–326.
[257] C.-C. Hu, C.-T. Hsu, K.-H. Chang, H.-Y. Hsu, J. Power Sources 238 (2013) 180–189.
[258] G. Chen, S.S. Liaw, B. Li, Y. Xu, M. Dunwell, S. Deng, H. Fan, H. Luo, J. Power Sources 251 (2014) 338–343.